Structure-Based Design of *N*-Phenyl Phenoxazine Transthyretin Amyloid Fibril Inhibitors

H. Michael Petrassi,‡ Thomas Klabunde,† James Sacchettini,† and Jeffery W. Kelly*,‡

Contribution from the Department of Chemistry and The Skaggs Institute of Chemical Biology, The Scripps Research Institute, 10550 North Torrey Pines Rd, MB12, La Jolla, California 92037, and Department of Biochemistry and Biophysics, Texas A&M University, College Station, Texas 77843

Received September 13, 1999

Abstract: Starting with the published 2.0 Å X-ray crystal structure of the transthyretin·(flufenamic acid)$_2$ complex, a simple structure-based ligand design strategy was employed to conceive of *N*-phenyl phenoxazine transthyretin (TTR) amyloid fibril inhibitors. Fifteen *N*-phenyl phenoxazines were chemically synthesized and evaluated using a quantitative amyloid fibril assay in vitro. The structure of one of the two most active phenoxazines, **4**, bound to TTR was solved to a resolution of 1.9 Å to understand the structural basis of its efficacy. *N*-phenyl phenoxazine **4** binds similar to the orientation anticipated, although not as deeply into the channel as expected. Like flufenamic acid, **4** mediates binding-induced conformational changes that enable intersubunit H-bonding in tetrameric TTR which may be important for preventing fibril formation. Analytical ultracentrifugation analysis demonstrates that **4** blocks the first step of TTR amyloid fibril formation, that is, tetramer dissociation to the alternatively folded amyloidogenic monomer. Isothermal titration calorimetry was used to determine the binding constants of **4** to TTR and to dissect the enthalpy and entropy contributions associated with ligand binding. Phenoxazine **4** exhibits binding and inhibitor efficacy against WT TTR that is very similar to that of flufenamic acid, unlike the situation with the inhibition of L55P fibril formation where **4** is superior to Flu as an inhibitor but not as a binder. It is clear that **4** functions in part by stabilizing the normally folded tetramer through formation of the TTR·(**4**)$_2$ complex, which in turn increases the activation energy for tetramer dissociation. The data also suggest that **4** destabilizes the transition state associated with TTR dissociation to the monomeric amyloidogenic intermediate. Future biophysical studies, including kinetic measurements, are needed to understand the exact mechanism(s) of the action of **4**.

Transthyretin (TTR) functions as the backup carrier of thyroxine (T4) in plasma and the main carrier of retinol binding protein.[1−6] In unfortunate individuals, plasma TTR is converted into amyloid fibrils in the extracellular space via misfolding and self-assembly, a process we have been able to simulate in vitro.[7−11] The self-assembly of transthyretin into amyloid fibrils is implicated as the cause of two amyloid diseases, senile systemic amyloidosis (SSA) and familial amyloid polyneuropathy (FAP). Wild-type (WT) transthyretin deposition is the putative cause of SSA, a late onset amyloid disease (80 years of age) associated with cardiac dysfunction,[12,13] whereas, fibril formation from one of >70 single site variants of TTR is genetically linked to pathology in FAP, which refers to a collection of early onset diseases characterized by neurodegeneration and/or organ dysfunction.[14−21]

Transthyretin is a 127-residue, β-sheet rich, homotetrameric protein (3.6 μM in plasma) that dissociates under acidic conditions from its normal quaternary structure to an alternatively folded monomeric amyloidogenic intermediate.[7−11,22−25] This intermediate self-assembles into protofilaments, filaments, and, under certain conditions, amyloid fibrils that render the

* To whom correspondence should be addressed. Telephone: (858) 784-9605. Fax: (858) 784-9610. E-mail: jkelly@scripps.edu.
† Texas A&M University.
‡ The Scripps Research Institute.

(1) Blake, C. C. F.; Geisow, M. J.; Oatley, S. J. *J. Mol. Biol.* **1978**, *121*, 339−356.
(2) Monaco, H. L.; Rizzi, M.; Coda, A. *Science* **1995**, *268*, 1039−1041.
(3) Pages, R. A.; Robbins, J.; Edelhoch, H. *Biochemistry* **1973**, *12*, 2773−2780.
(4) Ferguson, R. N.; Edelhoch, H.; Saroff, H. A.; Robbins, J. *Biochem.* **1975**, *14*, 282−289.
(5) Wojtczak, A.; Luft, J.; Cody, V. *J. Biol. Chem.* **1992**, *267*, 353−357.
(6) Wojtczak, A.; Cody, V.; Luft, J. R.; Pangborn, W. *Acta Crystallogr.* **1996**, *D52*, 758−765.
(7) Colon, W.; Kelly, J. W. *Biochemistry* **1992**, *31*, 8654−8660.
(8) McCutchen, S.; Colon, W.; Kelly, J. W. *Biochemistry* **1993**, *32*, 12119−12127.
(9) McCutchen, S. L.; Lai, Z.; Miroy, G.; Kelly, J. W.; Colon, W. *Biochemistry* **1995**, *34*, 13527−13536.
(10) Lai, Z.; Colon, W.; Kelly, J. W. *Biochemistry* **1996**, *35*, 6470−6482.
(11) Lashuel, H. A.; Lai, Z.; Kelly, J. W. *Biochemistry* **1998**, *37*, 17851−17864.
(12) Cornwell, G. C.; Sletten, K.; Johansson, B.; Westermark, P. *Biochem. Biophys. Res. Comm.* **1988**, *154*, 648−653.
(13) Westermark, P.; Sletten, K.; Johansson, B.; Cornwell, G. G. *Proc. Natl. Acad. Sci. U.S.A.* **1990**, *87*, 2843−2845.
(14) Jacobson, D. R.; Buxbaum, J. N. *Adv. Hum. Genet.* **1991**, *20*, 69−123.
(15) Jacobson, D. R.; Pastore, R. D.; Yaghoubian, R.; Kane, I.; Gallo, G.; Buck, F. S.; Buxbaum, J. N. *N. Engl. J. Med.* **1997**, *336*, 466−73.
(16) Benson, M. D. *TIBS* **1989**, *12*, 88−92.
(17) Coelho, T. *Curr. Opin. Neurol.* **1996**, *9*, 355−359.
(18) Saraiva, M. J. M.; Costa, P. P.; Goodman, D. S. *J. Lab. Clin. Med.* **1983**, *102*, 590−603.
(19) Saraiva, M. J. M.; Costa, P. P.; Goodman, D. S. *Adv. Neurol.* **1988**, *48*, 189−200.
(20) Sousa, A.; Coelho, T.; Barros, J.; Sequeiros, J. *Am. J. Med. Genet.* **1995**, *60*, 512−521.
(21) Saraiva, M. J. M. *Hum. Mutat.* **1995**, *5*, 191−196.
(22) Kelly, J. W. *Curr. Op. Struct. Biol.* **1996**, *6*, 11−17.
(23) Kelly, J. W. *Structure* **1997**, *5*, 595−600.
(24) Kelly, J. W. *Curr. Opin. Struct. Biol.* **1998**, *8*, 101−106.
(25) Lashuel, H.; Wurth, C.; Woo, L.; Kelly, J. W. *Biochemistry* **1999**, *38*, 13560−13573.

10.1021/ja993309v CCC: $19.00
Published on Web 02/23/2000

solution turbid.[11,25] The rate-determining step of TTR amyloid fibril formation appears to be tetramer dissociation.[26] Biophysical studies on WT TTR and the FAP-associated variants demonstrate a direct relationship between tetramer stability and the age of disease onset.[8,9,11,22−24,27−29] For example, the FAP-associated variant L55P exhibits disease onset at the earliest age (~20 yr) and has been demonstrated to be the least stable TTR tetramer.[8,9,11,14,25,26] In fact, the L55P TTR tetramer is the only FAP-associated variant that dissociates to the monomeric amyloidogenic intermediate and forms amyloid protofilaments under physiological conditions (37 °C, pH 7.6).[11,25]

The amyloid hypothesis states that the process of amyloid fibril formation (involving numerous assembly intermediates) triggers the neurodegeneration and related pathology characterizing these diseases. The genetic evidence favoring this hypothesis is strong, but unambiguous proof and a mechanistic understanding of the pathology at the cell biology level are lacking.[14,15,30,31] A strategy in which small molecule binding is employed to prevent the deleterious conformational changes leading to amyloid fibril formation would be an ideal and stringent test of this hypothesis, particularly if the small molecule inhibited the initial misfolding step.[32,33] Misfolding appears to be the key step in amyloidogenesis in about half of the amyloid diseases, including those based on the assembly of transthyretin, lysozyme, and the immunoglobulin light chains.[22,23,34] The key to testing the small molecule inhibitor strategy in vivo is to develop a compound that exhibits high selectivity and binding affinity for TTR in plasma. Transthyretin's natural ligand, thyroid hormone, is not a good candidate due to its biological activity and high affinity for thyroid binding globulin (K_d 63 pM). However, studies employing WT TTR (3.6 μM) under acidic (pH 4.4) amyloid-forming conditions demonstrate that T4 (10.8 μM) stabilizes >95% of the TTR tetramer against amyloid fibril formation in vitro.[32] Two molecules of T4 bind TTR with negative cooperativity, facilitating intersubunit contacts that lower the free energy of the TTR·$(T4)_2$ complex (K_{d1} = 44 nM, K_{d2} = 2.08 μM). Stabilization of the tetramer by T4 shifts the equilibrium toward tetramer under amyloid forming conditions and increases the activation barrier for tetramer dissociation to the alternatively folded monomeric amyloidogenic intermediate, thus inhibiting TTR amyloid fibril formation.[32]

Previously published screening efforts identified several compounds as potent TTR amyloid fibril inhibitors including flufenamic acid (Flu).[33,35−37] This anthranilic acid stabilizes the tetramer and prevents WT, V30M, and L55P TTR amyloid fibril formation at pH 4.4, a pH that normally yields the maximal quantity of amyloid fibrils.[33] A published 2.0 Å crystal structure of the TTR·$(Flu)_2$ complex reveals that Flu nicely complements the van der Waals surface of the two hormone binding sites in TTR, Figure 1, A and B.[33] A rearrangement in the TTR structure induced by placement of the phenyl substituent in the inner binding cavity and the *m*-CF_3 group in the deepest halogen binding pocket reorients the Ser-117 and Thr-119 side chains from their conformations in apo TTR or the TTR·$(T4)_2$ structures, and in the process displaces an ordered H_2O molecule.[33] The ligand binding mediated TTR conformational change reorients the Ser-117 side chains to a more interior position where the side chains in all four subunits are close enough to form a desolvated intersubunit hydrogen bonding network that is thought to stabilize the TTR tetramer, Figure 1, A and B.[33]

The transthyretin tetramer, which possesses 222 molecular symmetry, is constructed from identical monomers in nearly identical conformations assembled around the central ligand binding channel (see Figure 6 for a depiction of the tetramer with two ligands bound to the central channel). The crystallographic 2-fold axis (*Z*-axis, Figure 1A) running through the channel transforms two identical dimers composing each binding site. The other 2 perpendicular 2-fold axes (*X* and *Y*) are not crystallographic; instead they transform subunits that are nearly identical, only differing slightly in the conformation of the loop regions exposed on the surface of the tetramer. The occupancy of both ligand binding sites by Flu appears to be required to achieve nearly complete TTR amyloid fibril inhibition with this ligand, Table 1 and Figure 3B. It is difficult to saturate both ligand binding sites because Flu binds with negative cooperativity, Table 2.[33] In addition, many of the FAP-associated variants (e.g., L55P) bind Flu with 2−4-fold lower affinity at both the first and second sites relative to WT TTR (Table 2) making amyloid fibril inhibition of these variants even more difficult.[4,33,38] If 2 equiv of ligand (7.2 μM) turns out to be generally required for complete inhibition of TTR amyloidogenesis, then non- or positively cooperative ligand binding behavior is desired. An ideal small molecule inhibitor would prevent TTR fibril formation at a tetramer to ligand stoichiometry of 1:1, that is, at a concentration of 3.6 μM.

The anthranilic acid substructure of Flu occupies only about 50% of the outer TTR thyroid hormone binding cavity in each C_{2z} symmetry equivalent binding mode, Figure 1, A and B. Hence, an inhibitor that simultaneously occupies both sites should bind TTR with higher affinity and selectivity.[33] The substituted phenoxazines envisioned by the structure-based design approach outlined within prove to be excellent TTR amyloid fibril inhibitors, especially against the most pathogenic FAP-associated variant L55P. The approach used here is very similar to that in one of the first manuscripts on structure-based ligand design by Blaney and Blake, who used the TTR·$(T4)_2$ structure to design α-naphthyl thyroid hormone analogues.[39]

Experimental Section

General Methods. Unless otherwise stated reagents were purchased from commercial suppliers and used without further purification. All reactions were carried out under an argon atmosphere in flame-dried glassware. Reaction progress was monitored by thin-layer chromatography on silica gel 60 F_{254} coated aluminum plates (EM sciences). All flash chromatography was performed using 230−400 mesh silica gel 60, (EM Sciences). NMR spectra were recorded either at 300, 400,

(26) Lai, Z.; McCulloch, J.; Kelly, J. W. *Biochemistry* **1997**, *36*, 10230−10239.
(27) Nettleton, E. J.; Sunde, M.; Lai, Z.; Kelly, J. W.; Dobson, C. M.; Robinson, C. V. *J. Mol. Biol.* **1998**, *281*, 553−564.
(28) Alves, I. L.; Altland, K.; Almeida, M. R.; Winter, P.; Saraiva, M. J. *Hum. Mutat.* **1997**, *9*, 226−233.
(29) Quintas, A.; Saraiva, M. J. M.; Brito, R. M. M. *FEBS Lett.* **1997**, *418*, 297−300.
(30) Selkoe, D. J. *J. Biol. Chem.* **1996**, *271*, 18295−18298.
(31) Selkoe, D. J. *Science* **1997**, *275*, 630−631.
(32) Miroy, G. J.; Lai, Z.; Lashuel, H.; Peterson, S. A.; Strang, C.; Kelly, J. W. *Proc. Natl. Acad. Sci. U.S.A.* **1996**, *93*, 15051−15056.
(33) Peterson, S. A.; Klabunde, T.; Lashuel, H. A.; Purkey, H.; Sacchettini, J. C.; Kelly, J. W. *Proc. Natl. Acad. Sci. U.S.A.* **1998**, *95*, 13407−13412.
(34) Jarrett, J.; Lansbury, P. T. *Cell* **1993**, *73*, 1055−1058.
(35) Baures, P. W.; Peterson, S. A.; Kelly, J. W. *Bioorg. Med. Chem.* **1998**, *6*, 1389−1401.
(36) Baures, P. W.; Oza, V. H.; Peterson, S. A.; Kelly, J. W. *Bioorg. Med. Chem.* **1999**, *7*, 1339−1347.
(37) Oza, V. B.; Petrassi, H. M.; Purkey, H. E.; Kelly, J. W. *Bioorg. Med. Chem. Lett.* **1999**, *9*, 1−6.
(38) Almeida, M., R. Saraiva, Maria J. *Eur. J. Endocrinol.* **1996**,*135*, 226−230.
(39) Blaney, J. M.; Jorgensen, E. C.; Connolly, M. L.; Ferrin, T. E.; Langridge, R.; Oatley, S. J.; Burridge, J. M.; Blake, C. C. F. *J. Med. Chem.* **1982**, *25*, 785−790.

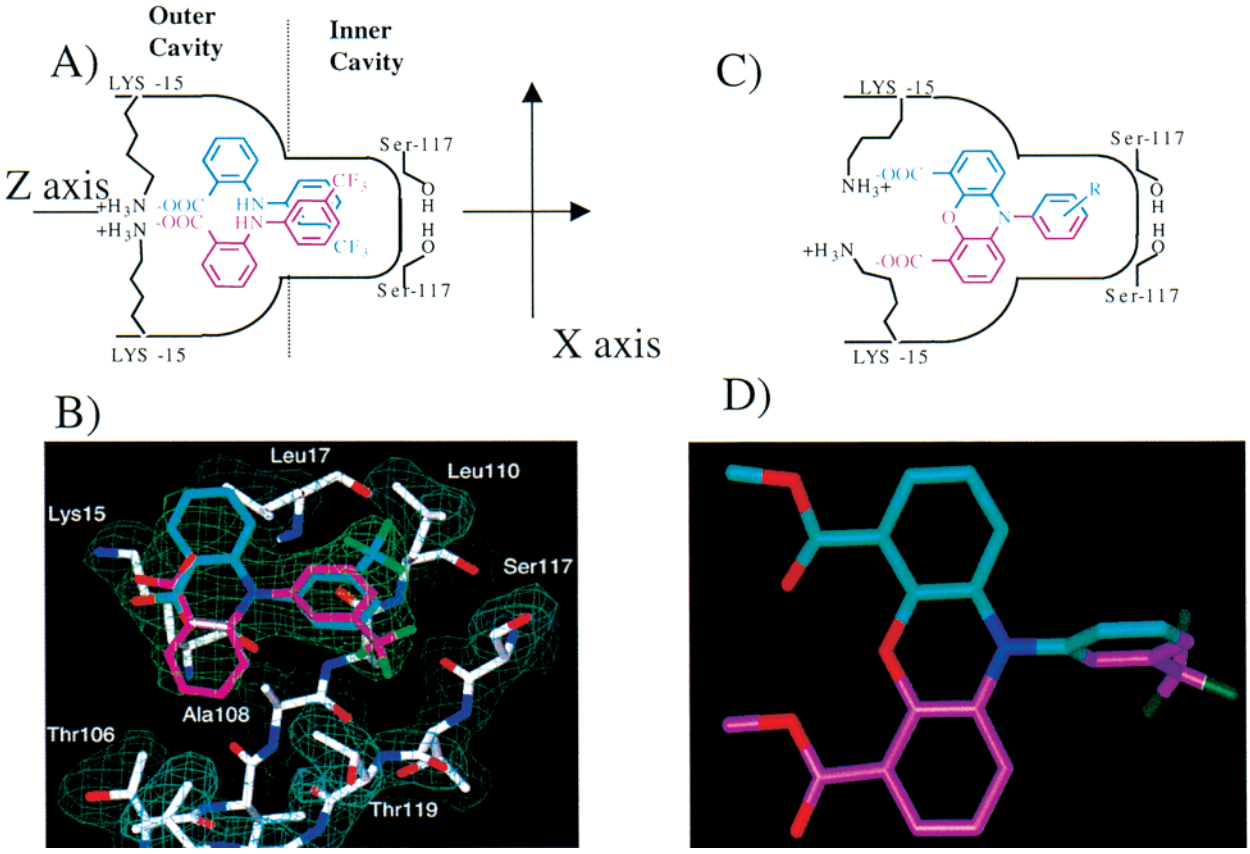

Figure 1. (A) A simplified representation of one of the two C_{2x} symmetrical TTR ligand binding sites. The crystallographic 2-fold axis (*Z*-axis) running through the center of the ligand binding channel transforms two identical dimers composing the tetramer, each set forming a ligand binding site (one set shown). The occupancy of one site by Flu is depicted in both of its C_{2z} symmetry equivalent binding modes, one in blue, one in maroon.[33] For a view of both C_{2x} symmetrical TTR ligand binding sites bound to **4** see Figure 6. (B) A framework model representing both C_{2z} symmetry equivalent binding modes of Flu along with their collective electron density (same color scheme as in A) generated by the $2|F_o| - |F_c|$ Φ_{calc} map with a σ of 2 at 2.0 Å resolution (shown in green) suggest that a tricyclic ring system would nicely occupy all of the conformational space traced out by Flu in the outer binding cavity. (C) A simplified representation of the anticipated binding mode of the N^{10}-phenyl phenoxazine-4,6-dicarboxylate inhibitors conceived of by the structure-based ligand design approach described within. The N^{10}-phenyl ring projects into the inner binding cavity whereas the phenoxazine ring system occupies the outer cavity. (D) Framework structural model representing the solid-state structure of **22** (the diester of **4**) derived from the X-ray crystal coordinates (Supporting Information Table 1).

500, or 600 MHz on Bruker spectrometers. In the spectral data, t* refers to an apparent triplet where the separation between the center resonance and the left and the right wings are slightly different, suggesting second-order contributions; the *J* values given refer to those separations. Chemical shifts are reported in parts per million downfield from the internal standard (Me_4Si, 0.0 ppm). Reverse phase high performance liquid chromatography (HPLC) was carried out on a Waters 600E multi-solvent delivery system employing a Waters 486 tunable absorbance detector (λ_{det} = 323 nm). A C18 Vydac column was employed for preparative work (model 218TP1022 300-Å, 5-μ pore size, 22 mm i.d. by 250 mm) and for ananlytical studies (model 218TP54 300-Å, 5-μ pore size, 4.6 mm i.d. by 250 mm). A gradient of CH_3CN was used to elute the phenoxazine-based compounds off the reverse phase column. A linear increase in the B solvent (95% CH_3CN, 4.8% H_2O, 0.2% TFA) relative to solvent A (95% H_2O, 4.8% CH_3CN, 0. 2% TFA) at a flow rate of 10 mL/min for preparative and 1.0 mL/min for analytical columns was employed.

10-(*tert*-Butyldimethylsilyl)-phenoxazine (1). Compound **1** was prepared by using the modified procedure of Antonio et al.[40] A 1 L flame-dried round-bottom flask equipped with a septum-capped reflux condenser was charged with a dry stir bar and phenoxazine (10.93 g, 60 mmol) and was evacuated (high vacuum). The flask was flame-dried and then back-filled with argon. Anhydrous THF (600 mL) was added to the flask by cannulation, and the flask was cooled to 0 °C (ice/H_2O bath). Solid NaH (3.6 g, 90 mmol, 1.5 equiv) was added by momentarily breaking the connection to the flask and condenser under a positive argon flow. The ice/H_2O bath was replaced with an oil bath, and the reaction was heated to reflux for 1 h (upon heating the reaction mixture, a large evolution of gas was observed). The oil bath was removed, and the flask was allowed to cool to room temperature. A solution of *tert*-butyldimethylsilyl chloride (1 M solution in THF, 90 mL, 90 mmol, 1.5 equiv) was cannulated through the septum. An oil bath was then used to reflux the reaction for 6 h. After removal of the oil bath the reaction mixture was poured into 1 L of a distilled ice/H_2O slurry in a 3 L separatory funnel that was extracted with EtOAc (4 × 400 mL). The organic layers were combined and dried with $MgSO_4$. The solvent was then removed under reduced pressure to afford a light-brown solid residue. The crude product was purified by flash chromatography (900 mg of SiO_2, 5% EtOAc in hexanes, R_f = 0.84) to afford 13.69 g (77%) of **1** as a white solid; ^{1}H NMR (500 MHz, $CDCl_3$) δ 0.35 (s, 6H), 1.06 (s, 9H), 6.94−7.01 (m, 8H); ^{13}C NMR (125 MHz, $CDCl_3$) δ −2.57, 20.12, 27.54, 116.03, 121.93, 123.06, 123. 22, 136.90, 151.44; FABMS (NBA/NaI) *m/z* 297 (M^+ requires $C_{16}H_{23}NOSi$ requires 297).

10-(*tert*-Butyldimethylsilyl)-phenoxazine-4,6-dimethyldicarboxylate (2). Compound **2** was prepared by using the modified procedure of Antonio et al.[40] A 1 L flame-dried round-bottom flask was equipped with a stirbar, charged with **1** (17.6 g, 59.1 mmol), septum-capped, and evacuated. The flask was flame-dried and back-filled with argon.

(40) Antonio, Y.; Barrera, P.; Contreras, O.; Franco, F.; Galeazzi, E.; Garcia, J.; Greenhouse, R.; Guzman, A.; Velarde, E. *J. Org. Chem.* **1989**, *54*, 2159−2165.

Table 1: Structural Summary of the N^{10}-phenyl-4,6-phenoxazine Dicarboxylic Acid Based Amyloid Fibril Formation Inhibitors[a]

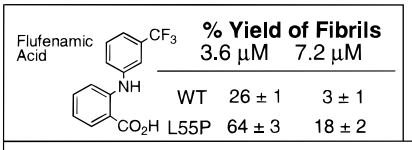

	% Yield of Fibrils 3.6 μM	7.2 μM
WT	26 ± 1	3 ± 1
L55P	64 ± 3	18 ± 2

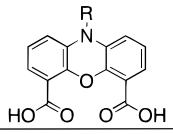

#	R		% Yield of Fibrils 3.6 μM	7.2 μM
4		WT	21 ± 2	2 ± 1
		L55P	43 ± 4	2 ± 3
5		WT	26 ± 1	2 ± 2
		L55P	52 ± 3	2 ± 1
6		WT	29 ± 2	12 ± 10
		L55P	61± 3	28 ± 4
7		WT	34 ± 6	10 ± 10
		L55P	65 ± 4	19 ± 3
8		WT	34 ± 6	3 ± 2
		L55P	58 ± 5	7 ± 2
9		WT	37 ± 2	3 ± 1
		L55P	55 ± 4	6 ± 3
10		WT	40 ± 3	3 ± 1
		L55P	63 ± 3	12 ± 7
11		WT	58 ± 3	31 ± 11
		L55P	92 ± 2	65 ± 3
12		WT	68 ± 7	46 ± 8
		L55P	95 ± 5	77 ± 4
13		WT	68 ± 3	48 ± 4
		L55P	90 ± 4	77 ± 2
14		WT	70 ± 3	48 ± 2
		L55P	92 ± 5	80 ± 2
15		WT	78 ± 3	50 ± 3
		L55P	90± 5	71 ± 2
16		WT	80 ± 2	73 ± 11
		L55P	98 ± 2	94 ± 3
17		WT	81 ± 1	66 ± 8
		L55P	98 ± 2	93 ± 5
18		WT	83 ± 11	46 ± 2
		L55P	100 ± 5	96± 2
19		WT	100 ± 5	78 ± 6
		L55P	100 ± 5	96 ± 4
20		WT	95 ± 3	79 ± 6
		L55P	100 ± 5	100 ± 4

[a] Accompanying the structures are the corresponding yields of fibrils formed from WT and L55P TTR at pH 4.4 in the presence of 3.6 or 7.2 μM inhibitor. When inhibitors are compared, percent conversion of tetrameric TTR into amyloid (oligomers, protofilaments, and filaments) over a 72 h period is reported relative to TTR lacking inhibitor (100%). Hence, 100% yield corresponds to no inhibition, and 0% corresponds to complete inhibition.

Table 2: Isothermal Titration Calorimetry Analysis of the Binding of Flu and **4** to WT and L55P TTR

(A) Dissociation Constants K_d Associated with the Binding of Inhibitors to Transthyretin[a]

	WT K_{d1}	WT K_{d2}	L55P K_{d1}	L55P K_{d2}
Flu	30 ± 13	255 ± 97	74 ± 16	682 ± 80
4	79 ± 18	237 ± 26	357 ± 30	1050 ± 80

(B) Thermodynamic Binding Parameters Associated with Inhibitor Binding to WT Transthyretin[b]

	ΔG_1	ΔH_1	$T\Delta S_1$	ΔG_2	ΔH_2	$T\Delta S_2$
Flu	−10.25 ± 0.25	−11.4 ± 0.7	−1.15 ± 0.75	−8.99 ± 0.22	−13.4 ± 0.7	−4.14 ± .73
4	−9.67 ± 0.14	−4.52 ± 0.4	5.15 ± 0.45	−9.03 ± 0.06	−5.18 ± 0.2	3.85 ± .24

(C) Thermodynamic Binding Parameters Associated with Inhibitor Binding to L55P Transthyretin[b]

	ΔG_1	ΔH_1	$T\Delta S_1$	ΔG_2	ΔH_2	$T\Delta S_2$
Flu	−9.72 ± 0.2	−11.2 ± 0.2	−1.48 ± 0.16	−8.40 ± 0.12	−13.4 ± 0.3	−5.0 ± 0.33
4	−8.79 ± 0.1	−6.3 ± 0.3	2.49 ± 0.33	−8.14 ± 0.05	−6.89 ± 0.3	1.25 ± 0.33

[a] Dissociation constants in nm units. [b] Binding free energies, enthalpies, and binding entropies resulting from an isothermal titration calorimetry analysis of Flu and **4** binding to WT (B) and L55P (C) TTR (ΔG, ΔH, and $T\Delta S$ values are reported in units of kcal/mol).

Anhydrous THF (626 mL) was cannulated through the septum, and the flask was cooled to 0 °C with an ice/H_2O bath. A solution of *n*-BuLi in hexanes (1.4 M, 140 mL, 200 mmol, 3.3 equiv) was cannulated through the septum. After addition, the cooling bath was removed, and the reaction was allowed to warm to room temperature and stir for 3 h. The flask was cooled to −78 °C with an acetone/dry ice slurry, and after 10 min gaseous CO_2 was added to the reaction solution via a submerged syringe needle at a pressure of 15 psi. The cooling bath was removed, and the reaction was allowed to stir and warm to room temperature over the course of 1 h. The reaction mixture was poured into a 2 L beaker containing an ice/H_2O slurry (500 mL). The solution pH was increased to 9 via the slow addition of 0.05 M KOH. The

solution was transferred to a 3 L separatory funnel and extracted with EtOAc (3 × 300 mL) to remove unreacted **1**. The aqueous solution was transferred to a beaker and cooled to 0 °C with an ice/H_2O bath. The solution was acidified to pH 2 with 0.5 M HCl precipitating a white solid. The aqueous suspension (pH 2) was transferred back into the 3 L separatory funnel, extracted with EtOAc (5 × 400 mL), and dried with $MgSO_4$. The organic layer was concentrated under reduced pressure in a 500 mL round-bottom flask to afford the crude diacid, an oil. The 500 mL flask containing the crude diacid was equipped with a stir bar, septum-capped and evacuated. The flask was flame-dried and then back-filled with argon. Anhydrous MeOH (160 mL) and ACS reagent grade benzene (40 mL) were added via cannulation. Trimethylsilyldiazomethane (2 M solution in hexanes, 148 mmol, 74 mL, 2.5 equiv) was added slowly via syringe through the septum. The reaction was then allowed to stir for 10 min and the solvent was removed under reduced pressure. The crude product was purified by flash chromatography (900 mg of SiO_2, 40% EtOAc in hexanes, $R_f = 0.63$) to afford 19.4 g (79%) of **2** as a yellow solid; ^{1}H NMR (500 MHz, $CDCl_3$) δ 0.17 (s, 6H), 1.02 (s, 9H), 3.94 (s, 6H), 6.93−7.01 (m, 4H), 7.37 (d, J = 7.7 Hz, 2H); ^{13}C NMR (125 MHz, $CDCl_3$) δ −3.27, 19.76, 27.63, 52.09, 120.47, 122.86, 124.89, 125.02, 137.49, 150.25, 165.80; FABMS (NBA/NaI) m/z 413 (M^+ requires $C_{20}H_{27}NOSi$ requires 413).

Phenoxazine-4,6-dimethyldicarboxylate (3). Compound **3** was prepared by using the modified procedure of Antonio et al.[40] A 500 mL round-bottom flask equipped with a stir bar was charged with **2** (17.9 g, 43 mmol), septum-capped, and evacuated. The flask was flame-dried and back-filled with argon. Anhydrous THF (100 mL) was cannulated through the septum. Tetrabutylammonium fluoride (1 M in THF, 65 mL, 65 mmol, 1.5 equiv) was added to the reaction via syringe. The reaction was stirred for 1 h at room temperature and then poured into 300 mL of H_2O in a 2 L separatory funnel. Compound **3** was extracted with EtOAc (3 × 200 mL). The organic layers were combined and dried with $MgSO_4$, and the solvent was removed under reduced pressure. The product residue was recrystallized from hexanes:EtOAc (9:1) to afford 11.24 g (87%) of **3** as a yellow crystalline solid. ^{1}H NMR (600 MHz, DMSO-d_6) δ 3.80 (s, 6H), 6.63 (dd, J = 1.7, 7.9 Hz, 2H), 6.83 (t, J = 7.9 Hz, 2H), 6.89 (dd, J = 1.7, 7.9 Hz, 2H), 8.64, (s, 1H); ^{13}C NMR (150 MHz, DMSO d_6) δ 52.03, 116.15, 119.49, 121.08, 124.03, 132.98, 141.21, 165.46; FABMS (NBA/NaI) m/z 299 (M^+ requires $C_{25}H_{23}NO_5$ requires 299).

General Procedure for the Synthesis of *N*-Phenyl Phenoxazines. The aryl coupling procedure utilized was that reported by Buchwald and Hartwig.[41,42] A flame-dried 10 mm × 13 cm borosilicate tube, equipped with a stirbar and septum-capped, was charged with **3** (400 mg, 1.3 mmol), palladium dibenzylidene acetone, $Pd_2(dba)_3$ (61 mg, 0.06 mmol, 0.05 equiv), (±)-Binap (62 mg, 0.08 mmol, 0.075 equiv), Cs_2CO_3 (645 mg, 1.82 mmol, 1.4 equiv), and the aryl halide or triflate (1.6 mmol, 1.2 equiv). In the case of nonvolatile reagents, the reaction tube was evacuated for 1 h and back-filled with argon. In the case of a volatile reagent the flask was simply purged with argon. In both cases, anhydrous toluene (2.4 mL) was added through the septum, and the reaction mixture was heated to 100 °C for 36 h in an oil bath. The reaction mixture was filtered through a cellulose paper filter, and the solid residue was washed with CH_2Cl_2 (3 × 10 mL). The solvent was removed under reduced pressure, and the resulting crude compounds were purified by flash chromatography.

10-(*m*-Trifluoromethylphenyl)-phenoxazine-4,6-dimethyldicarboxylate (21). A mixture of 3-bromobenzotrifluoride (400 μL, 1.6 mmol) and **3** (400 mg, 1.33 mmol) was subjected to the general coupling procedure outlined above. The crude product was purified by flash chromatography (150 mg of SiO_2 20% EtOAc in hexanes, $R_f = 0.35$) to afford 118 mg (26%) of **21** as a bright-yellow solid; ^{1}H NMR (300 MHz, $CDCl_3$) δ 3.94 (s, 6H), 5.96 (d, J = 7.9 Hz, 2H), 6.66 (m, 2H), 7.11 (d, J = 7.9 Hz, 2H), 7.11 (d, J = 7.9 Hz, 2H), 7.50−7.83 (m, 4H); ^{13}C NMR (75 MHz, $CDCl_3$) δ 52.13, 115.93, 119.98, 123.24, 125.06, 125.87, 132.16, 134.07, 134.39, 142.76, 165.67; MALDIHRMS (DHB) m/z 446.0874 ((M + Na)$^+$, $C_{23}H_{16}F_3NO_5Na$ requires 446.0878).

10-(*m*-Isopropylphenyl)-phenoxazine-4,6-dimethyldicarboxylate (22). A mixture of 3-isopropylphenyl triflouromethanesulfonate **37** (400 μL, 1.6 mmol) and **3** (400 mg, 1.33 mmol) were subjected to the general coupling procedure outlined above. The crude product was purified by flash chromatography (150 mg of SiO_2, 20% EtOAc in hexanes, $R_f = 0.39$) to afford 252 mg (45%) of **22** as a bright yellow solid. ^{1}H NMR (600 MHz, $CDCl_3$) δ 1.28 (d, J = 7.0 Hz, 6H), 2.97 (heptet, J = 7.0 Hz, 1H), 3.91 (s, 6H), 6.00 (d, J = 7.9 Hz, 2H), 6.60 (t, J = 7.9 Hz, 2H), 7.05 (d, J = 7.5 Hz, 2H), 7.08 (d, J = 7.9 Hz, 1H), 7.14 (s, 1H), 7.35 (d, J = 7.5 Hz, 2H), 7.51 (t, J = 7.9 Hz, 1H); ^{13}C NMR (150 MHz, $CDCl_3$) δ 23.78, 33.85, 52.02, 115.98, 119.56, 122.45, 122.93, 126.92, 127.34, 128.07, 131.09, 134.75, 138.24, 142.79, 152.62, 165.85; FABHRMS (NBA/CsI) m/z 417.1563 ($M^{\cdot+}$, $C_{25}H_{23}NO_5$ requires 417.1576).

10-(3,5-Bis-trifluoromethylphenyl)-phenoxazine-4,6-dimethyldicarboxylate (23). A mixture of 3,5 bis-trifluoromethyl bromobenzene (470 mg, 329 μL, 1.6 mmol) and **3** (400 mg, 1.33 mmol) was subjected to the general coupling procedure outlined above. The crude product was purified by flash chromatography (150 mg of SiO_2, 20% EtOAc in hexanes, $R_f = 0.34$) to afford 132 mg (26%) of **23** as a bright yellow solid. ^{1}H NMR (400 MHz, $CDCl_3$) δ 3.96 (s, 6H), 5.96 (dd, J = 7.9, 1.4 Hz, 2H), 6.71 (t, J = 7.9 Hz, 2H), 7.18 (dd, J = 7.9, 1.4 Hz, 2H), 7.86 (s, 2H), 8.04 (s, 1H) ^{13}C NMR (100 MHz, $CDCl_3$) δ 52.26, 116.07, 120.44, 122.90, 123.32, 123.87, 124.06, 131.64, 133.54, 134.98, 135.32, 140.71, 142.96, 165.52; FABHRMS (NBA/CsI) m/z 643.9889 ((M + Cs)$^+$, $C_{24}H_{15}F_6NO_5Cs$ requires 643.9909).

10-(*p*-Methylbenzoate)-phenoxazine-4,6-dimethyldicarboxylate (24). A mixture of methyl 4-bromobenzoate (346 mg, 1.6 mmol) and **3** (400 mg, 1.33 mmol) were subjected to the general coupling procedure outlined above. The crude product was purified by flash chromatography (150 mg of SiO_2, 20% EtOAc in hexanes, $R_f = 0.35$) to afford 255 mg (44%) of **24** as a bright yellow solid; ^{1}H NMR (500 MHz, $CDCl_3$) δ 3.91 (s, 6H), 3.98 (s, 3H), 6.00 (d, J = 8.1 Hz, 2H), 6.63 (t*, J = 7.7, 8.1 Hz, 2H), 7.10 (d, J = 7.7 Hz, 2H), 7.41 (d, J = 8.5 Hz, 2H), 8.29 (d, J = 8.5 Hz, 2H); ^{13}C NMR (125 MHz, $CDCl_3$) δ 51.85, 52.10, 112.96, 115.85, 119.61, 122.84, 130.32, 132.40, 133.74, 142.48, 142.54, 161.06, 165.36, 165.62; FABHRMS (NBA/CsI) m/z 434.1229 (M+H$^+$, $C_{24}H_{20}NO_7$ requires 434.1240).

10-(*m*-Ethylphenyl)-phenoxazine-4,6-dimethyldicarboxylate (25). A mixture of 3-ethylphenyl triflouromethanesulfonate **36** (400 μL, 1.6 mmol) and **3** (400 mg, 1.33 mmol) was subjected to the general coupling procedure outlined above. The crude product was purified by flash chromatography (150 mg of SiO_2, 20% EtOAc in hexanes, $R_f = 0.31$) to afford 401 mg (74%) of **25** as a bright yellow solid; ^{1}H NMR (500 MHz, $CDCl_3$) δ 1.24 (t, J = 7.4 Hz, 3H), 2.69 (q, J = 7.4 Hz, 2H), 3.93 (s, 6H), 6.00 (d, J = 8.1 Hz, 2H), 6.56 (t*, J = 8.1, 7.9 Hz, 2H), 7.02−7.10 (m, 4H), 7.29 (d, J = 7.4 Hz, 1H), 7.48 (t, J = 7.7 Hz, 1H); ^{13}C NMR (125 MHz,$CDCl_3$) δ 15.23, 28.49, 52.00, 116.02, 119.54, 122.46, 122.90, 127.25, 128.35, 129.39, 131.07, 134.69, 138.24, 142.76, 147.86, 165.82; FABHRMS (NBA/CsI) m/z 403.1420 (M^+, $C_{24}H_{21}NO_5$ requires 403.1420).

10-(*m*-*tert*-Butylphenyl)-phenoxazine-4,6-dimethyldicarboxylate (26). A mixture of 3-*tert*-butylphenyl triflouromethanesulfonate (400 μL, 1.6 mmol) and **3** (400 mg, 1.33 mmol) was subjected to the general coupling procedure outlined above. The crude product was purified by flash chromatography (150 mg of SiO_2, 20% EtOAc in hexanes, $R_f = 0.31$) to afford 285 mg (49%) of **26** as a bright-yellow solid. ^{1}H NMR (400 MHz, $CDCl_3$) δ 1.31 (s, 9H), 3.96 (s, 6H), 5.90 (dd, J = 8.1, 1.6 Hz, 2H), 6.52 (t*, J = 8.1, 7.8 Hz, 2H), 6.95−6.97 (m, 2H), 6.97−7.01 (m, 1H), 7.18−7.20 (m, 1H), 7.42 (m, 2H); ^{13}C NMR (75 MHz, $CDCl_3$) δ 31.16, 34.83, 52.04, 116.00, 119.54, 122.46, 122.95, 125.76, 127.00, 130.84, 134.83, 138.03, 142.80, 155.04, 165.87; FABHRMS (NBA/CsI) m/z 454.1644 ((M + Na)$^+$, $C_{26}H_{25}NO_5Na$ requires 454.1630).

10-(*p*-Methyphenyl)-phenoxazine-4,6-dimethyldicarboxylate (27). A mixture of 4-bromotoluene (274 mg, 197 μL, 1.6 mmol) and **3** (400 mg, 1.33 mmol) was subjected to the general coupling procedure outlined above. The crude product was purified by flash chromatography (150 mg of SiO_2, 30% EtOAc in hexanes, $R_f = 0.48$) to afford 362 mg (70%) of **27** as a bright yellow solid; ^{1}H NMR (500 MHz, $CDCl_3$) δ 2.45 (s, 3H), 3.93 (s, 6H), 6.00 (dd, J = 8.1, 1.5 Hz,

(41) Wolfe, J. P.; Buchwald, S. L. *Tetrahedron Lett.* **1997**, *38*, 6359−6362.

(42) Louie, J.; Driver, M. S.; Hamann, B. C.; Hartwig, J. F. *J. Org. Chem.* **1997**, *62*, 1268−1273.

2H), 6.60 (t*, J = 8.1, 7.7 Hz, 2H), 7.04 (dd, J = 7.7, 1.5 Hz, 2H), 7.16 (d, J = 8.1 Hz, 2H), 7.39 (d, J = 8.1 Hz, 2H); ^{13}C NMR (75 MHz,$CDCl_3$) δ 21.26, 52.16, 116.11, 119.67, 122.57, 123.02, 130.13, 132.01, 134.72, 135.68, 138.98, 142.92, 166.03; FABHRMS (NBA/CsI) m/z 412.1161 ($(M + Na)^+$, $C_{23}H_{19}NO_5Na$ requires 412.1146).

10-(*p*-Nitrophenyl)-phenoxazine-4,6-dimethyldicarboxylate (28). A mixture of 4-nitrophenyl trifluoromethanesulfonate (434 mg, 1.6 mmol) and **3** (400 mg, 1.33 mmol) was subjected to the general coupling procedure outlined above. The crude product was purified by flash chromatography (150 mg of SiO_2, 20% EtOAc in hexanes, R_f =0.37) to afford 496 mg (99%) of **28** as a bright yellow solid; ^{1}H NMR (500 MHz, $CDCl_3$) δ 3.94 (s, 6H), 6.10 (dd, J = 7.7, 1.5 Hz, 2H), 6.69 (t, J = 8.1 Hz, 2H), 7.16 (dd, J = 7.7, 1.5 Hz, 2H), 7.55 (d, J = 8.8 Hz, 2H), 8.47 (d, J = 8.8 Hz, 2H); ^{13}C NMR (125 MHz, $CDCl_3$) δ 52.16, 116.59, 120.20, 123.14, 123.79, 126.60, 131.09, 133.44, 143.15, 144.93, 147.20, 165.46; FABHRMS (NBA/CsI) m/z 421.1036 ($(M + H)^+$, $C_{22}H_{17}N_2O_7$ requires 421.1048).

10-(*p*-Cyanophenyl)-phenoxazine-4,6-dimethyldicarboxylate (29). A mixture of 4-bromobenzonitrile (291 mg, 1.6 mmol) and **3** (400 mg, 1.33 mmol) was subjected to the general coupling procedure outlined above. The crude product was purified by flash chromatography (150 mg of SiO_2, 30% EtOAc in hexanes, R_f = 0.33) to afford 110 mg (20%) of **29** as a bright-yellow solid; ^{1}H NMR (500 MHz, $CDCl_3$) δ 3.93 (s, 6H), 6.02 (d, J = 8.1 Hz, 2H), 6.67 (t*, J = 7.7, 8.1 Hz, 2H), 7.14 (d, J = 8.1 Hz, 2H), 7.49 (d, J = 8.1 Hz, 2H), 7.93 (d, J = 8.1 Hz, 2H); ^{13}C NMR (125 MHz, $CDCl_3$) δ 52.21, 112.76, 116.26, 117.75, 120.23, 123.14, 123.63, 131.52, 133.61, 135.23, 142.96, 143.11, 165.58; FABHRMS (NBA/CsI) m/z 400.1069 (M^+, $C_{23}H_{16}N_2O_5$ requires 400.1059).

10-(*p*-Methoxyphenyl)-phenoxazine-4,6-dimethyldicarboxylate (30). A mixture of 4-iodoanisole (278 mg, 1.2 mmol), palladium (II) acetate (7 mg, 0.025 mmol), Cs_2CO_3 (456 mg, 1.4 mmol), dioxane (2 mL), (+)-(*S*)-1-[(*R*)-2-(diphenylphosphino)ferrocenyl] ethyl methyl ether (50 mg, 0.05 mmol), and **3** (298 mg, 1.0 mmol) was charged into a flame-dried 10 mL round-bottom flask equipped with a stir bar and a septum-capped reflux condenser. The reaction mixture was heated for 24 h at reflux with an oil bath and then worked up according to the general procedure. The crude product was purified by flash chromatography (150 mg of SiO_2, 30% EtOAc in hexanes, R_f = 0.44) to afford 110 mg (20%) of **30** as a bright-yellow solid; ^{1}H NMR (500 MHz, $CDCl_3$) δ 3.79 (s, 3H), 3.88 (s, 6H), 5.92 (dd, J = 8.1, 1.5 Hz, 2H), 6.61 (t, J = 8.1 Hz, 2H), 6.95 (dd, J = 8.1, 1.5 Hz, 2H), 7.00 (d, J = 8.8 Hz, 2H), 7.10 (d, J = 8.8 Hz, 2H); ^{13}C NMR (125 MHz,$CDCl_3$) δ 52.04, 55.43, 116.00, 116.40, 119.57, 122.46, 122.95, 130.37, 131.38, 135.00, 142.82, 159.53, 165.89; FABHRMS (NBA/CsI) m/z 428.1128 ($M + Na^+$, $C_{23}H_{19}NO_6Na$ requires 428.1110).

10-(*m*-Methylphenyl)-phenoxazine-4,6-dimethyldicarboxylate (31). A mixture of 3-methylphenyl trifluoromethanesulfonate **35** (400 μL, 1.6 mmol) and **3** (400 mg, 1.33 mmol) was subjected to the general coupling procedure outlined above. The crude product was purified by flash chromatography (150 mg of SiO_2, 20% EtOAc in hexanes, R_f = 0.31) to afford 319 mg (63%) of **31** as a bright yellow solid; ^{1}H NMR (300 MHz, $CDCl_3$) δ 2.41 (s, 3H), 3.96 (s, 6H), 6.00 (d, J = 7.9 Hz, 2H), 6.60 (t, J = 7.9 Hz, 2H), 7.02−7.10(m, 4H), 7.29 (d, J = 7.5 Hz, 1H), 7.48 (m, 1H); ^{13}C NMR (75 MHz, $CDCl_3$) δ 21.23, 52.02, 116.02, 119.51, 122.46, 122.89, 127.08, 129.59, 130.98, 131.27, 134.65, 138.14, 141.49, 142.74, 165.81; FABHRMS (NBA/NaI) m/z 412.1146 (M^+, $C_{23}H_{19}NO_5Na$ requires 412.1161).

10-(*p*-trifluoromethylphenyl)-phenoxazine-4,6-dimethyldicarboxylate (32). A mixture of 4-iodobenzotrifluoride (435 mg, 235 μL, 1.6 mmol) and **3** (400 mg, 1.33 mmol) was subjected to the general coupling procedure outlined above. The crude product was purified by flash chromatography (150 mg of SiO_2, 20% EtOAc in hexanes, R_f = 0.32) to afford 119 mg (19%) of **32** as a bright-yellow solid; ^{1}H NMR (600 MHz, $CDCl_3$) δ 3.93 (s, 6H), 5.98 (dd, J = 7.9, 1.7 Hz, 2H), 6.63 (t, J = 7.9 Hz, 2H), 7.10 (dd, J = 7.9, 1.7 Hz, 2H), 7.47 (d, J = 8.3 Hz, 2H), 7.88 (d, J = 8.3 Hz, 2H); ^{13}C NMR (150 MHz, $CDCl_3$) δ 52.13, 116.02, 120.02, 123.08, 123.23, 128.51, 131.26, 133.98, 141.96, 142.78, 165.67; FABHRMS (NBA/NaI) m/z 466.0868 ($M + Na^+$, $C_{23}H_{16}F_3NO_5Na$ requires 466.0878).

10-(Phenyl)-phenoxazine-4,6-dimethyldicarboxylate (33). A mixture of bromobenzene (350 μL, 1.6 mmol) and **3** (400 mg, 1.33 mmol) was subjected to the general coupling procedure outlined above. The crude product was purified by flash chromatography (150 mg of SiO_2, 20% EtOAc in hexanes, R_f = 0.29) to afford 223 mg (48%) of **33** as a bright-yellow solid; ^{1}H NMR (500 MHz, $CDCl_3$) δ 3.81 (s, 6H), 5.88 (dd, J = 8.1, 1.5 Hz, 2H), 6.50 (t*, J = 8.1, 7.7 Hz, 2H), 6.95 (dd, J = 7.7, 1.5 Hz, 2H), 7.18 (m, 2H), 7.39 (m, 1H), 7.50 (m, 2H); ^{13}C NMR (125 MHz, $CDCl_3$) δ 52.00, 115.96, 119.60, 122.55, 122.91, 128.84, 130.32, 131.26, 134.60, 138.29, 142.72. 165.76; FABHRMS (NBA/NaI) m/z 375.1107 (M^+, $C_{22}H_{17}NO_5$ requires 375.1099).

10-(*m*-Trifluoromethylpyrimidine)-phenoxazine-4,6-dimethyldicarboxylate (34). A mixture of 2 chloro-4-trifluoromethyl pyrimidine (657 mg, 434 μL, 3.2 mmol) and **3** (400 mg, 1.33 mmol) was subjected to the general coupling procedure outlined above. The crude product was purified by chromatography (150 mg of SiO_2, 20% EtOAc in hexanes, R_f = 0.33) to afford 239 mg (41%) of **34** as a slightly yellowish solid; ^{1}H NMR (500 MHz, $CDCl_3$) δ 4.01 (s, 6H), 7.18 (d, J = 4.8 Hz, 1H), 7.23 (t*, J = 7.7, 8.1 Hz, 2H), 7.68 (dd, J = 7.7, 1.5 Hz, 2H), 7.94 (dd, J = 8.1, 1.5 Hz, 2H), 8.63 (d, J = 4.78 Hz, 1H); ^{13}C NMR (125 MHz, $CDCl_3$) δ 52.31, 110.09, 121.25, 122.67, 128.14, 130.23, 150.39, 159.13, 160.28, 165.35; FABHRMS (NBA/NaI) m/z 445.0876 (M^+, $C_{22}H_{17}NO_5$ requires 445.0886).

General Procedure for Ester Hydrolysis. Basic saponification was performed by dissolving methyl esters **21**−**35** in a THF:MeOH:H_2O (3:1:1) ternary solvent system in a round-bottom flask equipped with a stir bar. To each 1 equiv of methyl ester was added 4 equiv of LiOH, and the reaction was allowed to stir until complete (typically 4 h) as determined by TLC or analytical reverse phase HPLC monitoring. The reaction mixtures were poured into a separatory funnel and acidified to pH 2 with 1 M HCl (pH paper). The diacids were extracted with EtOAc, $CHCl_3$, or a mixture of thereof. In cases where purification was necessary, compounds were purified either by recrystallization (EtOAc/hexanes), flash chromatography, or by reverse phase HPLC.

10-(*m*-Trifluoromethylphenyl)-phenoxazine-4,6-dicarboxylate (4). Dimethyl ester **21** (303 mg, 0.683 mmol) was subjected to the ester hydrolysis procedure outlined above. The crude product was dissolved in DMSO and purified by reverse phase HPLC, employing a linear gradient of 20−80% B over 25 min to yield 277 mg of **4** (98%); ^{1}H NMR (600 MHz DMSO-d_6) δ 5.98 (dd, J = 7.9, 1.5 Hz, 2H), 6.78 (t, J = 7.9 Hz, 2H), 7.11 (dd, J = 7.9, 1.5 Hz, 2H), 7.82−7.94 (m, 1H), 7.97−8.03 (m, 3H); ^{13}C NMR (150 MHz, DMSO-d_6) δ 117.10, 120.51, 123.79, 124.74, 126.87, 128.11, 134.77, 136.27, 142.68, 166.52; FABHRMS (NBA/NaI) m/z 415.0668 (M^+ requires $C_{25}H_{23}NO_5$ requires 415.0678).

10-(*m*-Isopropylphenyl)-phenoxazine-4,6-dicarboxylate (5). Dimethyl ester **22** (100 mg, 0.24 mmol) was subjected to the ester hydrolysis procedure outlined above. Extraction afforded 90 mg of pure **5** (96%); R_f = 0.38 (0.1% TFA, 39.9% EtOAc in hexanes) ^{1}H NMR (600 MHz, DMSO-d_6) δ 1.24 (d, J = 7.0 Hz, 6H), 2.96 (heptet, J = 7.0 Hz, 1H), 5.97 (d, J = 7.9 Hz, 2H), 6.74 (t, J = 7.9 Hz, 2H), 7.09 (d, J = 7.9 Hz, 2H), 7.21 (d, J = 7.9 Hz, 1H), 7.28 (s, 1H), 7.43 (d, J = 7.9 Hz, 2H), 7.59 (t, J = 7.9 Hz, 1H); ^{13}C NMR (150 MHz, DMSO-d_6) δ 23.75, 33.31, 116.23, 119.38, 122.70, 123.89, 127.18, 127.32, 127.86, 131.53, 134.34, 137.81,141.93, 152.49, 165.68; MALDIFTMS (DHB) 412.1165 m/z ($(M + Na)^+$,$C_{23}H_{19}NO_5Na$ requires 412.1161).

10-(3,5-Bis-trifluoromethylphenyl)-phenoxazine-4,6-dicarboxylate (6). Dimethyl ester **23** (150 mg, 0.293 mmol) was subjected to the ester hydrolysis procedure outlined above. Extraction afforded 140 mg of pure **6** (99%); R_f = 0.41 (0.1% TFA, 39.9% EtOAc in hexanes); ^{1}H NMR (600 MHz, DMSO-d_6) δ 6.04 (d, J = 7.9 Hz, 2H), 6.77 (t, J = 7.9 Hz, 2H), 7.13 (d, J = 7.5 Hz, 2H), 8.34 (s,1H), 8.38 (s, 2H); ^{13}C NMR (150 MHz, DMSO-d_6) δ 116.54, 119.85, 121.96, 123.34, 123.87, 132.78, 133.71, 140.31, 141.94, 165.67; MALDIFTMS (DHB) 483.0556 m/z (M^+ requires $C_{22}H_{11}F_6NO_5$ requires 483.0541).

10-(*p*-Carboxyphenyl)-phenoxazine-4,6-dicarboxylate (7). Dimethyl ester **24** (225 mg, 0.519 mmol) was subjected to the ester hydrolysis procedure outlined above. Extraction afforded 200 mg of pure **7** (99%); R_f = 0.17 (0.1% TFA, 39.9% hexanes in EtOAc); ^{1}H NMR (500 MHz, DMSO-d_6) δ 6.05 (dd, J = 7.7, 1.5 Hz, 2H), 6.77 (t*, J = 8.1, 7.7 Hz, 2H), 7.11 (dd, J = 8.1, 1.3 Hz, 2H), 7.59 (d, J =

8.5 Hz, 2H), 8.22 (d, $J = 8.5$ Hz, 2H); ^{13}C NMR (150 MHz, DMSO-d_6) δ 116.31, 120.09, 123.15, 123.83, 130.61, 131.50, 132.62, 133.88, 141.95, 142.04, 165.68, 166.58; MALDIFTMS (DHB) 391.0684 *m/z* (M^+ requires $C_{21}H_{12}NO_7$ requires 391.0692).

10-(*m*-Ethylphenyl)-phenoxazine-4,6-dicarboxylate (8). Dimethyl ester **25** (100 mg, 0.25 mmol) was subjected to the ester hydrolysis procedure outlined above. Extraction afforded 93 mg of pure **8** (99%); $R_f = 0.17$ (0.1% TFA, 39.9% hexanes in EtOAc); ^{1}H NMR (600 MHz DMSO-d_6) δ 1.22 (t, $J = 7.7$ Hz, 3H), 2.70 (q, $J = 7.7$ Hz, 2H), 6.00 (d, $J = 8.1$ Hz, 2H), 6.76 (t, $J = 8.1$ Hz, 2H), 7.10 (d, $J = 8.1$ Hz, 2H), 7.28 (s, 1H), 7.24 (d, $J = 7.7$ Hz, 1H), 7.42 (d, $J = 7.7$ Hz 1H), 7.60 (t, $J = 7.7$ Hz, 1H); ^{13}C NMR (150 MHz, DMSO-d_6) δ 15.75, 29.36, 118.23, 124.52, 125.17, 128.33, 129.52, 130.43, 132.27, 135.53, 139.45, 144.06, 149.21, 165.09; MALDIFTMS (DHB) 398.1012 *m/z* ($(M + Na)^+$ requires $C_{22}H_{17}NO_5Na$ requires 398.1004).

10-(*m*-*tert*-Butylphenyl)-phenoxazine-4,6-dicarboxylate (9). Dimethyl ester **26** (100 mg, 0.2 mmol) was subjected to the ester hydrolysis procedure outlined above. Extraction afforded 91 mg of pure **9** (98%); $R_f = 0.16$ (0.1% TFA, 39.9% hexanes in EtOAc); ^{1}H NMR (600 MHz, DMSO-d_6) δ 1.31 (s, 9H), 5.98 (d, $J = 7.9$ Hz, 2H), 6.77 (t, $J = 7.9$ Hz, 2H), 7.09 (d, $J = 7.9$ Hz, 2H), 7.24 (d, $J = 7.0$ Hz, 1H), 7.43 (s, 1H), 7.59−7.64 (m, 2H); ^{13}C NMR (150 MHz, DMSO-d_6) δ 31.00, 34.74, 103.46, 116.14, 119.40, 122.61, 123.89, 125.95, 126.86, 126.98, 131.26, 134.41, 137.59, 141.91, 154.83, 165.67; MALDIFTMS (DHB) 426.1325 *m/z* ($(M + Na)^+$ requires $C_{24}H_{21}NO_5$-Na requires 426.1317).

10-(*p*-Methylphenyl)phenoxazine-4,6-dicarboxylate (10). Dimethyl ester **27** (150 mg, 0.385 mmol) was subjected to the ester hydrolysis procedure outlined above. Extraction afforded 129 mg of pure **10** (86%). $R_f = 0.51$ (0.1% TFA, 39.9% hexanes in EtOAc); ^{1}H NMR (500 MHz, DMSO-d_6) δ 2.42 (s, 3H), 6.00 (dd, $J = 8.1$, 1.5 Hz, 2H), 6.75 (t, $J = 8.1$ Hz, 2H), 7.07 (dd, $J = 8.1$, 1.5 Hz, 2H), 7.31 (d, $J = 8.4$ Hz, 2H), 7.50 (d, $J = 8.4$ Hz, 2H); ^{13}C NMR (150 MHz, DMSO-d_6) δ 21.70, 117.08, 120.35, 123.49, 124.70, 130.78, 133.05, 135.28, 136.04, 139.71, 142.69, 166.55; MALDIFTMS (DHB) 361.0941 *m/z* (M^+ requires $C_{24}H_{21}NO_5$ requires 361.0950).

10-(*p*-Nitrophenyl)phenoxazine-4,6-dicarboxylate (11). Dimethyl ester **28** (190 mg, 0.45 mmol) was subjected to the ester hydrolysis procedure outlined above. Extraction afforded 174 mg of pure **11** (98%). $R_f = 0.52$ (0.1% TFA, 39.9% hexanes in EtOAc); ^{1}H NMR (600 MHz, DMSO-d_6) δ 6.16 (d, $J = 7.9$ Hz, 2H), 6.80 (t, $J = 7.9$ Hz, 2H), 7.15 (d, $J = 7.9$ Hz, 2H), 7.78 (d, $J = 8.8$ Hz, 2H), 7.50 (d, $J = 8.8$ Hz, 2H); ^{13}C NMR (150 MHz, DMSO-d_6) δ 116.88, 120.24, 123.51, 123.84, 126.91, 131.55, 133.45, 142.23, 144.45, 147.15, 165.62; MALDIFTMS (DHB) 392.0647 *m/z* (M^+ requires $C_{20}H_{12}N_2O_7$ requires 392.0645).

10-(*p*-Cyanophenyl)phenoxazine-4,6-dicarboxylate (12). Dimethyl ester **29** (35 mg, 0.09 mmol) was subjected to the ester hydrolysis procedure outlined above. The crude product was dissolved in DMSO and purified by RP-HPLC employing a linear gradient of 50−100% B over (retention time = 12.1 min) 25 min to yield 29 mg of **12** (89%); ^{1}H NMR (600 MHz, DMSO-d_6) δ 6.07 (dd, $J = 8.1$, 1.5 Hz, 2H), 6.78 (t, $J = 8.1$ Hz, 2H), 7.13 (d, $J = 8.1$, 1.5 Hz, 2H), 7.72 (d, $J = 8.4$ Hz, 2H), 8.18 (d, $J = 8.4$ Hz, 2H); ^{13}C NMR (150 MHz, DMSO-d_6) δ 112.77,117.43, 119.14, 120.77, 124.05, 124.76, 132.58, 134.41, 136.69, 142.79, 143.40, 166.54; MALDIFTMS (DHB) 372.0753 *m/z* (M^+ requires $C_{21}H_{12}N_2O_5$ requires 372.0746).

10-(*p*-Methoxyphenyl)phenoxazine-4,6-dicarboxylate (13). Dimethyl ester **30** (28.2 mg, 0.069 mmol) was subjected to the ester hydrolysis procedure outlined above. Extraction afforded 25.1 mg of pure **13** (98%). $R_f = 0.50$ (0.1% TFA, 39.9% hexanes in EtOAc); ^{1}H NMR (600 MHz, DMSO-d_6) δ 3.84 (s, 3H), 6.00 (d, $J = 7.9$ Hz, 2H), 6.74 (t, $J = 7.9$ Hz, 2H), 7.06 (d, $J = 7.9$ Hz, 2H), 7.20 (d, $J = 8.8$ Hz, 2H), 7.33 (d, $J = 8.8$ Hz, 2H); ^{13}C NMR (150 MHz, DMSO-d_6) δ 55.48, 116.24, 116.76, 119.40, 122.61, 123.83, 130.10, 131.35, 134.64, 141.89, 159.35, 165.67; MALDIFTMS (DHB) 377.0893 *m/z* (M^+ requires $C_{21}H_{15}NO_6$ requires 377.0899).

10-(*m*-Methylphenyl)phenoxazine-4,6-dicarboxylate (14). Dimethyl ester **31** (100 mg, 0.26 mmol) was subjected to the ester hydrolysis procedure outlined above. Extraction afforded 91 mg of pure **14** (96%). $R_f = 0.51$ (0.1% TFA, 39.9% hexanes in EtOAc); ^{1}H NMR (500 MHz, DMSO-d_6) δ 2.40 (s, 3H), 6.01 (d, $J = 7.9$ Hz, 2H), 6.76 (t*, $J = 7.9$, 8.1 Hz, 2H), 7.09 (d, $J = 8.1$ Hz, 2H), 7.22 (d, $J = 7.7$ Hz, 1H), 7.26 (s, 1H), 7.39 (d, $J = 7.7$ Hz, 1H), 7.58 (t, $J = 7.7$ Hz, 1H); ^{13}C NMR (150 MHz, DMSO-d_6) δ 20.86, 116.29, 119.44, 122.64, 123.84, 126.99, 129.92, 130. 37, 131.41, 134.25, 137.78, 141.51. 141.82, 165.67; MALDIFTMS (DHB) 361.0963 *m/z* (M^+ requires $C_{24}H_{21}NO_5$ requires 361.0950).

10-(*p*-Phenol)phenoxazine-4,6 dicarboxylate (15). Dimethyl ester **30** (30 mg, 0.08 mmol) and a stir bar were added to a septum- capped 10 mL round-bottom flask. The flask was evacuated, flame-dried, and back-filled with argon. Anhydrous $CHCl_2$ (1.87 mL) was added to the flask via syringe. The flask was cooled to 0 °C with an ice/H_2O bath. A solution of BBr_3 (1 M, 1.11 mL, 1.11 mmol, 15 equiv) was added via syringe. The reaction was allowed to warm to room temp by removing the ice/H_2O bath and was stirred for 24 h. The reaction was quenched by the dropwise addition of H_2O (5 mL). The pH of the reaction mixture was increased to 10 via the addition of 1 M KOH and acidified to pH 2 via the addition of 1 M HCl. The acidified reaction mixture was then transferred to a 250 mL separatory funnel and extracted with $CHCl_3$ (3 × 50 mL). The organic layers were combined and dried with $MgSO_4$, and the solvent was removed under reduced pressure. Flash chromatography of the crude product (50 mg of SiO_2, 0.1% TFA, 39.9% hexanes in EtOAc, $R_f = 0.30$) yields 15.9 mg of pure **15** (60%); ^{1}H NMR (500 MHz, DMSO-d_6) δ 6.05 (d, $J = 8.1$ Hz, 2H), 6.76 (t*, $J = 7.7$, 8.1 Hz, 2H), 7.02 (d, $J = 7.7$ Hz, 2H), 7.08 (d, $J = 7.7$ Hz, 2H), 7.20 (d, $J = 7.7$ Hz, 2H); ^{13}C NMR (125 MHz, DMSO-d_6) δ 116.27, 117.97, 119.19, 122.49, 123.80, 128.45, 131.11, 134.73, 141.88, 157.76, 165.60; MALDIFTMS (DHB) 363.0747 *m/z* (M^+ requires $C_{24}H_{21}NO_5$ requires 363.0743).

10-(*p*-Trifluoromethylphenyl)phenoxazine-4,6-dicarboxylate (16). Dimethyl ester **32** (35 mg, 0.08 mmol) was subjected to the ester hydrolysis procedure outlined above. Extraction afforded 32 mg of pure **16** (98%). $R_f = 0.50$ (0.1% TFA, 39.9% hexanes in EtOAc); ^{1}H NMR (500 MHz, DMSO-d_6) δ 6.04 (d, $J = 7.7$ Hz, 2H), 6.78 (t*, $J = 7.7$, 8.1 Hz, 2H), 7.12 (d, $J = 8.1$ Hz, 2H), 7.73 (d, $J = 8.8$ Hz, 2H), 8.06 (d, $J = 8.8$ Hz, 2H); ^{13}C NMR (125 MHz, DMSO-d_6) δ 116.38, 119.81, 123.05, 123.85, 128.74, 128.95, 129.30, 129.56, 131.59, 133.68, 141.84, 165.60; MALDIFTMS (DHB) *m/z* 438.0548 ($(M + Na)^+$ requires $C_{21}H_{15}NO_6Na$ requires 438.0565).

10-(Phenyl)phenoxazine-4,6-dicarboxylate (17). Dimethyl ester **33** (17.1 mg, 0.05 mmol) was subjected to the ester hydrolysis procedure outlined above. The compound was dissolved in DMSO and purified by reverse phase HPLC, employing a linear gradient of 40−100% B over (retention time = 35.1 min) 55 min to yield 15 mg of **17** (98%). $R_f = 0.41$ (0.1% TFA, 39.9% hexanes in EtOAc); ^{1}H NMR (600 MHz, THF-d_8)δ 6.10 (d, $J = 7.9$ Hz, 2H), 6.72 (t*, $J = 7.9$, 8.1 Hz, 2H), 7.38−7.42 (m, 4H), 7.54 (t, $J = 7.5$ Hz, 1H), 7.68 (t, $J = 7.9$ Hz, 2H); ^{13}C NMR (125 MHz, DMSO-d_6) δ 116.19, 119.45, 122.68, 123.79, 129.23, 130.18, 131.63, 134.23, 137.84, 141.81, 165.59; MALDIFTMS (DHB) 370.0690 *m/z* ($(M + Na)^+$ requires $C_{21}H_{15}NO_6Na$ requires 370.0691).

10-(*tert*-butyldimethylsilyl)-phenoxazine-4,6-dicarboxylate (18). Crude **18** whose synthesis was described above was dissolved in DMSO and purified by reverse phase HPLC, employing a linear gradient of 40−100% B over (retention time = 35.1 min) 55 min, $R_f = 0.41$ (0.1% TFA, 39.9% hexanes in EtOAc); ^{1}H NMR (500 MHz, THF-d_8)δ 0.29 (s, 6H), 0.94 (s, 9H), 7.09 (t, $J = 7.7$ Hz, 2H), 7.19 (dd, $J = 7.4$, 1.6 Hz, 2H), 7.7 (dd, $J = 7.4$, 1.6 Hz, 2H); ^{13}C NMR (125 MHz, DMSO-d_6) δ −1.87, 20.75, 28.03, 117.61, 119.57, 121.32, 122.85, 124.65, 125.14, 125.88, 126.44, 133.54, 137.87, 142.37, 150.44, 166.32, 166.54; HRMS (NBA/CsI) *m/z* 386.1419 ($(M + H)^+$ requires $C_{20}H_{24}NO_5Si$ requires 386.1424).

Phenoxazine-4,6-dicarboxylate (19). The impure diacid **2** (114 mg, 0.29 mmol) (obtained before esterification with trimethylsilyl diazomethane) was added to a 500 mL flask with a stir bar. The flask was septum-capped, evacuated, flame-dried, and back-filled with argon. Anhydrous THF was cannulated through the septum. Tetrabutlyammonium fluoride (1 M in THF, 0.45 mL, 0.44 mmol, 1.5 equiv) was added to the reaction via syringe. After the reaction stirred for 1 h, it was poured into a 500 mL beaker containing 50 mL of H_2O. The contents of the beaker were transferred to a 250 mL separatory funnel and extracted with EtOAc (3 × 500 mL). The organic layers were

combined and dried with $MgSO_4$, and the solvent was removed under reduced pressure. The crude product was dissolved in DMSO and purified by reverse phase HPLC, employing a linear gradient of 40−100% B over (retention time = 35.1 min) 55 min to yield 45 mg of **19** (57%); ^{1}H NMR (400 MHz, DMSO-d_6) δ 6.65 (d, J = 7.6 Hz, 2H), 6.84 (t*, J = 7.6, 7.9 Hz, 2H), 7.03 (d, J = 7.9 Hz, 2H), 8.70 (s, 1H); ^{13}C NMR (100 MHz, DMSO-d_6) δ, 116.75, 118.74, 122.00, 124.29, 132.71, 141.53, 165.48; HRMS (DHB) m/z 294.0377 $(M + Na)^+$ requires $C_{14}H_9NO_5Na$ requires 294.0378).

10-(*m*-Trifluoromethylpyrimidine)-phenoxazine-4,6-dicarboxylate (20). Dimethyl ester **34** (17.1 mg, 0.05 mmol) was subjected to the ester hydrolysis procedure outlined above. The crude product was dissolved in DMSO and purified by reverse phase HPLC, employing a linear gradient of 50−100% B over (retention time = 15 min) 25 min to yield 15 mg of **20** (98%); ^{1}H NMR (400 MHz, DMSO-d_6) δ 7.32 (t, J = 7.9 Hz, 2H), 7.57 (d, J = 5.0 Hz, 1H), 7.62 (dd, J = 7.9, 1.5 Hz, 2H), 7.98 (dd, J = 7.9, 1.5 Hz, 2H), 8.86 (d, J = 5.0 Hz, 1H) ^{13}C NMR (100 MHz, DMSO-d_6) δ 111.01, 118.94, 121.95, 123.20, 127.68, 129.95, 149.35, 154.67, 158.77, 161.98, 165.52; MALDIFTMS (DHB) m/z 440.0466 $(M + Na)^+$ requires $C_{21}H_{15}NO_6Na$ requires 440.0466).

General Procedure for Phenol Triflation. The triflation procedure previously described by Stille et al., was used to synthesize all triflates from their respective phenols.[43] Briefly, a 10 mL round-bottom flask, fitted with a septum and a dry stir bar, was charged with the phenol (9 mmol), and distilled pyridine (3 mL, Aldrich, the solvent) via syringe through the septum. The reaction mixture was cooled to 0 °C with an ice/H_2O bath. To initiate the reaction trifluoromethane sulfonate anhydride (12 mmol, Aldrich) was then added via syringe through the septum. The ice bath was removed, and the reaction was allowed to warm to room temperature and stir overnight. The reaction mixture was then poured into a 250 mL beaker containing 50 mL of an ice/H_2O slurry. The contents of the beaker were transferred to a 125 mL separatory funnel, and the aqueous layer was extracted with Et_2O (3 × 35 mL). The organic layers were combined and dried over $MgSO_4$, and the solvent was removed under reduced pressure. The triflates were purified via flash chromatography from the resultant oil.

3-Methylphenyl Trifluoromethylsulfonate (35). *m*-Cresol (1 g, 1.54 mL, 9.2 mmol) was subjected to the general triflation procedure outlined above. The crude product was purified by chromatography (300 mg of SiO_2, 20% EtOAc in hexanes, R_f = 0.75) to afford 2.1 g (93%) of **35** as a pale yellow oil; ^{1}H NMR (600 MHz, $CDCl_3$) δ 2.34 (s, 3H), 7.02−7.07 (m, 2H), 7.15 (m, 1H), 7.27 (m, 1H); ^{13}C NMR (150 MHz,$CDCl_3$) δ 20.96, 118.12, 121.71, 129.11, 129.83, 140.92, 149.61; GCMS (electron ionization) m/z 240 ($C_8H_7F_3O_3S$ requires 240).

3-Ethylphenyl Trifluoromethylsulfonate (36). 3-Ethylphenol (1 g, 1.001 mL, 8.2 mmol) was subjected to the general triflation procedure outlined above. The crude product was purified by chromatography (300 mg of SiO_2, 20% EtOAc in hexanes, R_f = 0.79) to afford 1.81 g (87%) of **36** as a pale yellow oil; ^{1}H NMR (600 MHz, $CDCl_3$) δ 1.22 (t, J = 7.9 Hz, 3H), 2.67 (q, J = 7.9 Hz, 2H), 7.05−7.10 (m, 2H), 7.24 (m, 1H), 7.31 (m, 1H); ^{13}C NMR (150 MHz,$CDCl_3$) δ 15.00, 28.51, 118.36, 120.58, 127.92, 129.95, 147.24, 149.73; GCMS (electron ionization) m/z 254 ($C_9H_9F_3O_3S$ requires 254).

3-Isopropylphenyl Trifluoromethylsulfonate (37). 3-Isopropylphenol (0.994 g, 1.00 mL, 7.2 mmol) was subjected to the general triflation procedure outlined above. The crude product was purified by chromatography (300 mg of SiO_2, 5% EtOAc in hexanes, R_f = 0.43) to afford 1.33 g (69%) of **37** as a pale yellow oil; ^{1}H NMR (600 MHz, $CDCl_3$) δ 1.23 (d, J = 7.0 Hz, 6H), 2.91 (heptet, J = 7.0 Hz, 1H), 7.06 (d, J = 7.9 Hz, 1H), 7.11 (s, 1H), 7.22 (d, J = 7.9 Hz, 1H), 7.30 (t, J = 7.9 Hz, 1H); ^{13}C NMR (150 MHz,$CDCl_3$) δ 23.45, 33.94, 118.47, 119.24, 127.12, 129.98, 149.83, 151.98; GCMS (electron ionization) m/z 268 ($C_{10}H_{11}F_3O_3S$ requires 268).

Structure-Based Ligand Design. The structure of the TTR·$(Flu)_2$ complex served as a starting point for the design of inhibitory ligands. Visual inspection of the electron density traced out by both symmetry equivalent binding modes of Flu in the outer hormone binding cavity of TTR suggest that a tricyclic ring system would be ideal for occupancy of this cavity. Several computer modeling programs including the Biosym suite of software (Insight II), O, and manual docking algorithms were employed to identify tricyclic ring systems that have the appropriate geometry and van der Waals complimentarity.[39] Candidates including hetero-tricyclic ring systems, especially fused 6−6−6 and 6−5−6 systems were further scrutinized on the basis of which had the appropriate geometry and functionality coupled with applicable synthetic methodology to direct a phenyl substructure into the inner binding site. Another design feature considered was ease of synthesis for the introduction of the carboxylate substituents, such that electrostatic interactions with the Lys-15 ammonium groups in TTR could contribute to binding affinity. A few ring systems were identified, of which the phenoxazine class appeared ideal.

Sedimentation Velocity Analysis. All sedimentation analyses were performed on samples used previously for turbidity analysis, which measures the extent of amyloid fibril formation after 72 h or 7 days in 100 mM acetate buffer, 100 mM KCl, 1mM EDTA (pH 4.4).

Analysis of Sedimentation Velocity Profiles of TTR. The sedimentation properties of WT and L55P TTR solutions, in the presence and absence of inhibitors, were analyzed on a temperature controlled Beckman XL-I analytical ultracentrifuge equipped with a An60Ti rotor and a photoelectric scanner. Data were collected at speeds of 3000 and 50 000 rpm in continuous mode at 20 °C, employing a step size of 0.001 cm. Detection was carried out at 280 nm for samples incubated for 6 days and at 230 nm for the samples incubated for 3 days.

A direct boundary fitting approach was applied to evaluate the sedimentation velocity data derived from a 3.6 μM solution of TTR incubated with a 7.2 μM solution of **4** at pH 4.4. The Svedberg program was used to fit multiple concentration vs radial position data sets simultaneously to yield approximate solutions to the Lamm equation.[44] The fitting algorithm yields the sedimentation coefficient and diffusion coefficient which affords the molecular weight using equation I.

$$MW = sRT/D(1\text{-}\bar{v}\rho) \qquad \text{(I)}$$

In equation I, MW is the molecular weight in (Da), s is the sedimentation coefficient (in Svedberg units, 10^{-13} sec), R is the universal gas constant (8.314×10^7 erg/mol), $\bar{v}$ is the partial specific volume (cm^3 / g), and ρ is the solvent density (g/cm^3). The buffer density (1.00848 g/cm^3) was calculated from tabulated data. The partial specific volumes of WT (0.7346 cm^3/g) and L55P TTR (0.7334 cm^3/g) were calculated from the amino acid composition.[11]

Analysis of Sedimentation Equilibrium Properties of TTR under Fibril Formation Conditions in the Presence of Phenoxazine-Based Inhibitors. Sedimentation equilibrium measurements were made using 120−140 μL of TTR solution (3.6 μM) loaded into a double sector cell, equipped with a 12-mm Epon centerpiece and sapphire or quartz windows. Data were collected initially at rotor speeds of 3000 rpm to ensure the absence of large molecular weight oligomers (these would sediment) and then at 17 000 rpm to allow equilibrium to be established across the cell. The sedimentation profiles monitored (280 nm) at 3 h intervals were overlaid to establish that equilibrium had been achieved. Data analysis was carried out using a nonlinear least-squares analysis in the Origin software package provided by Beckman. Several different models including a single ideal species model and several multiple species models were fit to the data to identify the simplest model that best fits the data. Equation II corresponding to a single ideal species model fits the data best based on the small differences between the theoretical data and the experimental data:

$$A_r = \exp[\ \ln(A_o) + (M\omega^2(1-\bar{v}\rho/RT)(x^2 - x_o^2)] + E \qquad \text{(II)}$$

where A_r is the absorbance at radius x, A_o is the absorbance at a reference radius x_o (usually the meniscus), ω is the partial specific volume of the protein, ρ is the density of the solvent (g/cm^3), ω is the angular velocity of the rotor (radian/sec), E is the baseline error correction factor, M is the molecular weight, and R is the universal gas constant. The differences between the experimental data points and the fitted data

(43) Echavarren, A. M.; Stille, J. K. *J. Am. Chem. Soc.* **1987**, *109*, 5478−5486.

(44) Philo, S. J. In *Modern Analytical Ultracentrifugation;* Shuster, T. M., Laue, T. M., Eds.; Birkhäuser: Boston, 1994; pp 156−170.

points (the residuals) are randomly distributed and small in magnitude, other models did not fit the data well as discerned by the nonrandom distribution of residuals across the cell.

Fibril Formation Assay. Recombinant WT and L55P TTR were purified from *Escherichia coli* as described previously.[25] The stagnant amyloid fibril formation assay recently published by our laboratory was used to assess the efficacy of the phenoxazine-based amyloid fibril inhibitors.[10,32,35,36] Briefly, stock solutions of each inhibitor were prepared by dissolving the potential inhibitor in DMSO to a concentration of 7.2 mM (inhibitors were dried in a vacuum desiccator (<0.01 mmHg) for 12 h in the presence of phosphorus pentoxide and the solutions were made by weight). For assays in which the final inhibitor concentration was 7.2 or 3.6 μM, the initial 7.2 mM inhibitor stock solution was diluted to 1.4 mM and 720 μM solutions respectively with DMSO. A 7.2 μM TTR stock solution was prepared by dilution from a 3−5 mg/mL stock solution that had been dialyzed against a 10 mM phosphate buffer, 100 mM KCl, 1 mM EDTA (pH 7.6). The protein solution (495 μL) was delivered to Eppendorf tubes for each triplicate measurement, to which 5 μL of the inhibitor solution was added (except for the controls). Promising phenoxazines were tested at least three times in triplicate.

The inhibitor−TTR solutions were preincubated for 30 min at 37 °C to allow plenty of time for potential inhibitors to bind to TTR. The TTR solutions were rendered acidic and amyloidogenic by the addition of 500 μL of 200 mM acetate buffer, 100 mM KCl, 1 mM EDTA (pH 4.2), which was added to each TTR solution to yield a final pH of 4.4. These solutions were incubated for 72 h (37 °C) or a 7 day incubation (pH 4.4) to evaluate inhibitor efficacy. The Eppendorfs were vortexed for 5 s and their optical density at 400 nm measured to quantify fibril formation. The extent of TTR fibril formation in the absence of inhibitor was defined to be 100% (typically an o.d. between 1.15 and 1.25 for WT (60% chemical yield of fibrils), hence active inhibitors give <100% yield of fibrils. Inhibitors were tested in the absence of TTR to evaluate their intrinsic absorbance and to be sure that the inhibitor is soluble over the course of the assay (i.e. does not contribute to the turbidity, none of the phenoxazines show a o.d. > 0.05). Flufenamic acid (7.2 μM), (Table 2) was included as a positive control which typically yields 4 ± 5% of WT TTR fibril formation (95% inhibition).[33]

Structural Determination of 22 via X-ray Crystallography. A single parallelpiped shaped crystal of compound **22** was obtained by slow evaporation of a concentrated solution in $CHCl_3$/hexanes. The crystal was mounted along the largest dimension and data collected with a Rigaku AFC6R diffractometer equipped with a copper rotating anode and a highly orientated graphite monochromator. A constant scan speed of 8 °/min in a ω was used and weak reflections [$I > 5\sigma > I$] were rescanned a maximum of 6 times and the counts accumulated to ensure good counting statistics. The intensities of three monitored reflections measured after every 200 reflections did not change significantly during the 38 h of X-ray exposure. Unit cell dimensions and standard deviations were obtained by least-squares fit to 25 reflections ($80° < 2\Theta < 100°$). The data were corrected for Lorentz and polarization effects, but not for absorption because of low value of μ.

There were no systematic absences in the data, and therefore the space group $P\bar{1}$ was assumed and later confirmed by successful refinement of the structure. The structure was solved by direct methods using SHELX-97. All non-hydrogen atoms were refined anisotropically by the full matrix least-squares method. The function minimized was $\Sigma w\ (||F_o|| - ||F_c||^2)$. Hydrogen atoms were included in the ideal positions with fixed isotropic U values equal to 1.2 times that of the atom they are attached to. A weighting scheme of the form $w = 1/[\sigma(F_o^2) + (aP)^2 + bP]$ with $a = 0.0945$ and $b = 0.598$ was used. P is defined as Max $((F_o^2, 0) + 2F_c^2)/3)$. An extinction correction was also applied to the data. The refinement converged to the R indices given in supplemental Table 1. The final difference map was devoid of significant features.

All calculations were done on a Silicon graphics personal Iris 4D35 and an IBM-compatible PC using the program TEXSAN (data reduction), SHELX-97 (refinement), SHELXTL-PC (plotting) and CIFTAB to generate the tables. Final atomic coordinates and selected bond lengths and angles are tabulated in the Supporting Information Tables.

Table 3. Crystallographic Analysis of TTR·$(4)_2$ Complex[a]

resolution, Å	10−1.8
reflections, measured/unique	75643/22052
completeness, % overall/outer shell	95.3/97.5
$R_{sym,\%}$ overall/outer shell	4.4/17.3
I/σ_I	18.0
Refinement Statistics	
resolution, Å	8−1.9
completeness, %	82.4 ($F > 3\sigma$)
R_{factor}/R_{free}, %	20.2/20.3
rmsd bond length, Å	0.008
rmsd bond angle, deg	1.2327

[a] $R_{sym} = \Sigma|I - \langle I\rangle|/\Sigma\langle I\rangle$, where I is the observed intensity, and $\langle I\rangle$ is the average intensity of multiple observations of symmetry-related reflections. $R_{factor} = \Sigma||F_o| - |F_c||/\Sigma|F_o|$ where F_o and F_c are observed and calculated structure factor amplitudes, respectively.

X-ray Crystallographic Determination of the TTR·$(4)_2$ Complex. Crystals of recombinant TTR were grown from solutions of 5 mg/mL TTR (in 100 mM KCl, 100 mM phosphate, pH 7.4, 1 M ammonium sulfate) equilibrated against 2 M ammonium sulfate in hanging drop experiments. The complex of TTR with **4** was prepared from crystals soaked for 5 weeks with a 10-fold molar excess of the ligand to ensure full saturation of both binding sites. A DIP2030 imaging plate system (MAC Science, Yokohama, Japan) coupled to an RU200 rotating anode X-ray generator was used for data collection. Crystals of the TTR·$(4)_2$ complex are isomorphous with the native crystal form with unit cell dimensions in the range of $a = 43$ Å, $b = 86$ Å, and $c = 65$ Å. They belong to the space group $P2_12_12$, and contain one-half of the homotetramer in the asymmetric unit. Data were reduced with DENZO and SCALEPACK.

The protein atomic coordinates for apo TTR from the Protein Data Bank (accession number 1BMZ) were used as a starting model for the TTR·$(4)_2$ complex by molecular dynamics and energy minimization using the program CNS. Simulated annealing and individual temperature factor refinement provided a model that was used to phase the "complex-native" difference Fourier maps. In the resulting maps, the ligands could be located in both binding pockets of the TTR tetramer with peaks heights of above 7 σ_{rms}. At this point the ligand molecule was fit into the density found in both hormone binding cavities and was included into the crystallographic refinement. The conformation of the bis-methyl ester of **4**, **22**, determined by small molecule X-ray diffraction (Figure 1D, and Supporting Information) was in good agreement with the initial annealed 2 $|F_{o,complex}| - |F_{o,apo}|\ \Phi_{apo}$ maps and was used as initial conformation of **4** in the crystallographic refinement. Because of the 2-fold crystallographic axis along the binding channel, a statistical disorder model had to be applied, giving rise to two ligand binding modes in each of the two binding sites of tetrameric TTR. After several cycles of simulated annealing, subsequent positional and temperature factor refinement placed 60 H_2O molecules into the difference Fourier maps. For the TTR·$(4)_2$ complex both molecular conformations of **4** were in good agreement with unbiased annealed 2 $|F_o| - |F_c|\ \Phi_{calc}$ omit maps, phased in absence of the inhibitor. Because of the lack of interpretable electron densities in the final map, the 9 N-terminal and 3 C-terminal residues were not included in the final model. A summary of the crystallographic analysis can be found in Table 3. Coordinates for the TTR·$(4)_2$ complex have been deposited in the Brookhaven Protein Data Bank (accession numbers 1DVY).

Isothermal Titration Calorimetry. A filtered solution of **4** in 10 mM phosphate buffer, 100 mM KCl, 1 mM EDTA (pH 7.6) was titrated (25 °C) into a 1.3407 mL solution of TTR in the same buffer using a Microcal MCS isothermal titration calorimeter (Microcal Inc., Northampton, MD). Compound **4** was manipulated by dissolving reverse phase HPLC purified material into 5% ammonium carbonate solution which was lyophilized to afford the ammonium salt of **4**. The solution of **4** was then filtered through a 0.2 μ cellulose filter and its concentration determined by absorbance at 323 nM ($\epsilon = 6726\ M^{-1}\ cm^{-1}$). The TTR solution was prepared by dialysis of ~4 mg/mL solution against the

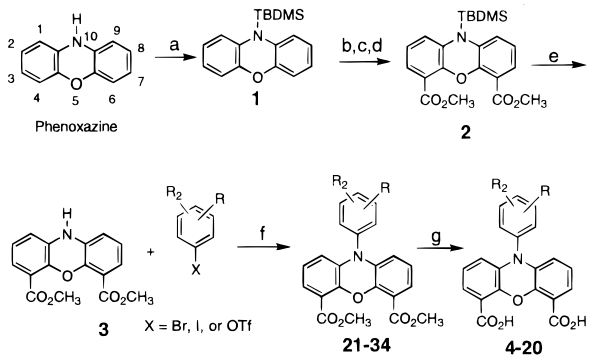

Figure 2. Summary of the key synthetic transformations in the synthesis of the N^{10}-phenyl-4,6-phenoxazine dicarboxylic acids; (a)-NaH, TBDMSCl, (b) *n*-BuLi, (c) gaseous CO_2, (d) $TMSCHN_2$, (e) TBAF, (f) $Pd_2(dba)_3$, Cs_2CO_3, (±)Binap, (g) LiOH or BBr_3.

same phosphate buffer, filtering as above. The final concentration was determined by absorbance at 280 nm. In the analysis of the binding of **4** to WT TTR (13.8 μM), the initial injection of 2 μL (530 μM) was followed by 24 injections of 8 μL, allowing a 4 min equilibration period between each injection. In the case of L55P TTR (23 μM) the initial injection of 2 μL of **4** (570 μM) was followed by 24 injections of 10 μL, with a 6 min equilibration period between injections. Three independent titrations for both WT and L55P TTR were performed. Two sets of blanks were also collected in triplicate, the first set of blanks being the titration of each solution of **4** into buffer (heat of dilution of the ligand) and the second being the titration of buffer into the respective protein solutions (heat of dilution of the protein). Integration of the thermogram and subtraction of all blanks gives a binding isotherm that fits to a model of two interacting sites exhibiting negative cooperativity. The data were fit by using the variables, K_1, H_1, K_2, and H_2 and the ITC Data Analysis Module in ORIGIN version 2.9 provided by Microcal.

Results

Design of Phenoxazines. The anthranilic acid substructure of Flu occupies only about 50% of the outer TTR thyroid hormone binding cavity in each symmetry equivalent binding mode, Figure 1, A and B. Consideration of the composite electron density (Figure 1B) occupied by both binding modes of Flu, (transformed by the crystallographic C_{2z} axis) suggests that a tricyclic ring system such as phenoxazine (Figure 1C) should fill the entire outer hormone binding cavity.[33] The geometry of phenoxazine appears to perfectly complement the van der Waals surface of the outer TTR binding cavity, which should lead to an increase in binding affinity and selectivity relative to Flu.[39] Furthermore, the N^{10} of phenoxazine (Figure 2) is ideally positioned to direct a substituted phenyl ring into the inner hormone binding cavity, Figure 1C. Hence, an N^{10}-phenyl phenoxazine appears optimal to fill both the outer and inner TTR binding cavities simultaneously, Figure 1C. All of the active inhibitors discovered by screening have carboxylate or phenolic substituents on the aromatic ring occupying the outer TTR binding cavity.[35−37,39,45] From unpublished crystallographic results and from the published TTR·$(Flu)_2$ structure outlined in the Introduction, we know that these acidic groups are ideally positioned to interact with the ϵ-ammonium groups of Lys-15, projecting into the periphery of the outer thyroid binding cavity from two adjacent TTR subunits.[33] Therefore, *N*-phenyl phenoxazines substituted with carboxylate groups at the 4- and 6-positions (Figure 2) should bind with high affinity due in part to these electrostatic interactions, Figure 1C. The *m*-CF_3 substituted phenyl ring of Flu nearly completely fills the van der Waals surface of the inner binding cavity of TTR, including one of the halogen binding pockets occupied by an iodine in the TTR·$(T4)_2$ structure.[33,39] Meta substituents on the inner phenyl ring should also mediate the Ser-117 side chain rearrangement described in the Introduction, which may stabilize the TTR tetramer, owing to intersubunit H-bonding.[33] Therefore *m*-substituted *N*-phenyl phenoxazines and related analogues were used to interrogate the inner TTR binding cavity in an effort to optimize the structure required to best stabilize the TTR tetramer against dissociation and tertiary structural changes required for amyloidogenesis.

Synthesis of Phenoxazines. The synthesis of the N^{10}-phenyl-4,6-phenoxazine dicarboxylic acids desired for this study commences with protection of N^{10} in commercially available phenoxazine, Figure 2. Following the procedure of Antonio et al., the anilino proton was removed by NaH and the N-centered anion silylated with *tert*-butyldimethyl silyl(TBDMS) chloride affording **1**.[40] The sterically demanding TBDMS group prevents N-directed metalation, allowing for selective oxygen directed ortho metalation at the 4,6-positions utilizing *n*-BuLi. Bis-lithiated phenoxazine was treated with gaseous CO_2, followed by esterification of the resulting dicarboxylic acid with trimethylsilyldiazomethane to yield the 4,6-dimethyl ester **2**. Removal of the *N*-silyl-protecting group with tetrabutylammonium fluoride generates anilino diester **3**. The anilino diester (N^{10}) was then coupled to a variety of aromatic iodides, bromides, or triflates using the Pd-mediated *N*-aryl coupling reactions developed by Buchwald and Hartwig, Figure 2 (see Table 1 for a summary of the analogues prepared). [41,42] In cases where the aryl triflate was not commercially available, it was prepared by treating the respective phenol with triflic anhydride in pyridine.[43] The methyl esters in compounds **21**−**29** and **31**−**34** were hydrolyzed using LiOH. In the case of **30**, where a methyl ether and methyl esters comprise the same molecule, the methyl-protecting groups were removed simultaneously by BBr_3 treatment.

Amyloid Fibril Inhibition. The extent of transthyretin amyloid fibril formation (from a 3.6 μM solution of either WT or L55P TTR at pH 4.4) in the presence of phenoxazine-based inhibitors **4**−**20** (3.6 or 7.2 μM) is reported in Table 1. The activities of compounds **4**−**6**, **17**, and for comparison purposes, flufenamic acid are represented in bar graph format in Figure 3 A and B. Compounds **4** and **5** were chosen because they are the best inhibitors, Flu is shown for comparative purposes as it is the lead molecule upon which the phenoxazine design was based. Compounds **6** and **17** were chosen for bar graph representation because they are similar in structure to **4** and **5**, but have surprisingly poor activity. When comparing inhibitors, percent conversion of tetrameric TTR into amyloid and its precursors (oligomers, protofilaments, filaments) over a 72 h period is reported relative to TTR lacking inhibitor (100%). Hence, 100% fibril formation reflects no inhibition, whereas 0% fibril formation is associated with complete amyloid fibril inhibition.

Phenoxazines **4** and **5** are better than Flu at inhibiting L55P TTR amyloid fibril formation, at a small molecule concentration of either 3.6 (Figure 3A) or 7.2 μM, Figure 3B. Compounds **4** and **5** are similar to Flu with respect to the inhibition of WT amyloid formation, Figure 3, A and B. Phenoxazines **6**−**10** are equal or better than Flu against the formation of L55P amyloid fibrils; however, 3.6 μM solutions of **6**−**10** are slightly inferior to Flu from the standpoint of inhibiting WT amyloidogenesis, Table 1. It is generally the case that meta-substitued *N*-phenylphenoxazines are superior to para-substitued *N*-phenyl phenoxazines, which are better than the unsubstituted *N*-phenyl phenoxazine, **17**, Table 1. The 4,6-phenoxazine dicarboxylate,

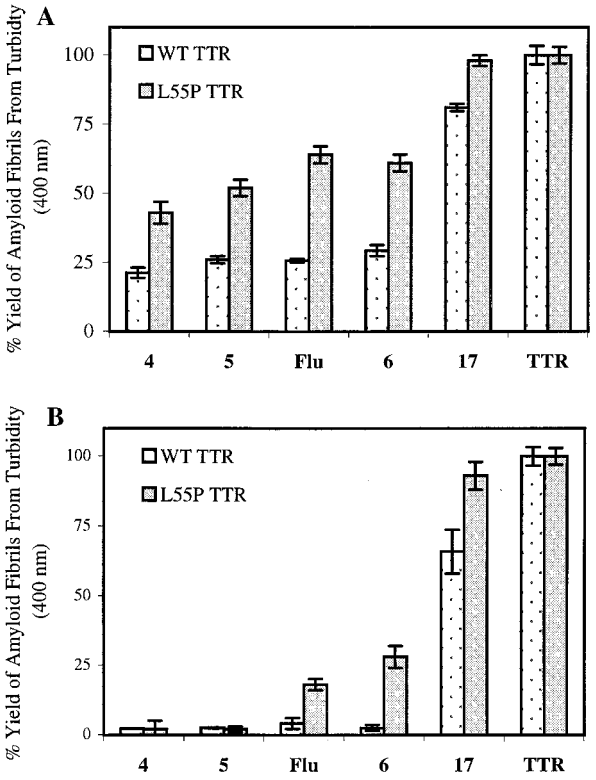

Figure 3. A bar graph representation of the relative yield of TTR amyloid precursors and fibrils produced from WT and L55P TTR (3.6 μM) at pH 4.4, after 72 h of incubation at 37 °C in the presence of either 3.6 (A) or 7.2 μM (B) concentration of inhibitor. When comparing inhibitors percent conversion of tetrameric TTR into amyloid is reported. Hence, 100% fibril yield reflects no inhibition, whereas a 0% fibril yield corresponds to complete inhibition.

19, is not by itself capable of significant amyloid fibril inhibition, demonstrating the importance of *N*-phenyl ring. An analogue of **6** lacking both carboxylate groups is also inactive as an inhibitor, even at a concentration of 36 μM (data not shown), demonstrating the importance of the electrostatic interactions for binding and inhibition. However, we know from **19** that these interactions alone are not sufficient for inhibition. Compound **20** is unique with respect to the other *N*-phenyl phenoxazines outlined in Table 1 in that the pyrimidine ring can rotate freely, relative to the phenoxazine ring system, Table 1. The conformational freedom exhibited by phenoxazine **20** did not improve biological activity; in fact, it is a very poor inhibitor, Table 1.

Binding Constant Determination. Isothermal titration calorimetry was employed to measure the binding constants of the phenoxazine-based TTR amyloid fibril inhibitor **4** and to evaluate the cooperativity or lack thereof between the TTR binding sites, Table 2. The raw isothermal titration calorimetry data and the fit to the isotherms for **4** binding to WT and L55P TTR can be found in Supporting Information, Figures 1 and 2, respectively. Phenoxazine **4** exhibits binding to WT TTR that is similar to that of flufenamic acid. The dissociation constant (K_{d1}) of **4** for the first site of WT TTR is 79 nM, (Table 2A) a 2-fold decrease in affinity relative to Flufenamic acid (K_{d1} = 30 nM). The binding affinities of **4** and Flu for the second site of WT TTR are within error (237 ± 26 vs 255 ± 97 nM), Table 2A. Hence, the negative cooperativity exhibited for Flu binding is not observed for 4 binding to TTR, as the ≈4-fold difference observed between K_{d1} and K_{d2} is that expected for the statistical effects of ligand binding to a protein with two identical sites (non-cooperative binding). In contrast to the similarities observed in the binding constants of **4** and Flu to WT TTR, **4** binds to the two sites of L55P TTR with decreased affinity in comparison to Flu. Phenoxazine **4** binds to the fist site of L55P with a K_{d1} of 357 nM. This is over 5 times the K_{d1} characterizing Flu binding to L55P. The differences in the dissociation constant of **4** and Flu binding to L55P TTR at the second site are not as dramatic (1.5-fold), Table 2A. The negative cooperativity associated with L55P ligand binding disappears when comparing Flu to **4**, very similar to the trend observed for WT TTR.

Dissection of the free energies associated with phenoxazine **4** and Flu binding to TTR reveals a noteworthy difference. Flufenamic acid binding to both sites in WT TTR is enthalpically driven, with the entropy associated with the binding and linked TTR conformational changes being unfavorable, Table 2B. On the contrary, there is a favorable entropic component for the binding and linked conformational changes associated with the interaction of **4** with WT TTR, Table 2B. The entropy term contributes 53% (5.15 of 9.67 kcal/mol) of the free energy for the first binding event and 43% (3.85 of 9.03 kcal/mol) of the free energy for the second binding event, the remaining contribution coming from enthalpy. A favorable entropy contribution to the free energy is also observed in the case of the binding of **4** to L55P TTR, (Table 2C) although in this case the enthalpy terms make the dominant contribution to the binding free energy.

Analytical Equilibrium Ultracentrifugation Studies. Sedimentation equilibrium and sedimentation velocity experiments evaluating the quaternary structure of WT and L55P TTR (3.6 μM) were performed with and without inhibitor **4** (7.2 μM), at a pH associated with maximal amyloid fibril formation (pH 4.4). WT TTR bound to **4** remains tetrameric after 72 h of incubation (pH 4.4) with no detectable loss of protein (<5%) according to sedimentation equilibrium studies, Figure 4A. The fit to a single ideal species model is excellent as evident from the small magnitude and random distribution of the residuals. The solution molecular weight from the single ideal species model is 51 513 ± 430 Da, in good agreement with the expected MW of the TTR tetramer (55 032 Da). WT TTR self-assembles into high MW oligomers that sediment from the cell in the absence of inhibitor (72 h of incubation, pH 4.4, 37 °C) at the same angular velocity (17 000 rpm) used for equilibrium experiments described directly above (data not shown). Similarly, in the absence of inhibitor **4**, L55P TTR (3.6 μM) forms large oligomers that sediment out of the cell (17 000 rpm) under amyloid fibril forming conditions (pH 4.4, 37 °C, 72 h) (data not shown). However, in the presence of inhibitor **4**, an equilibrium analysis (17 000 rpm) reveals retention of >95% of the tetrameric form of L55P TTR, even after 7 days of preincubation at pH 4.4, Figure 4B. The solution molecular weight from the ideal species model is 50 110 ± 476 Da, in very good agreement with the expected MW of the tetramer (54 982 Da). Sedimentation velocity studies of WT and L55P TTR (3.6 μM) preincubated for 6 days at pH 4.4 in the presence of a 7.2 μM solution of **4** also demonstrate that TTR remains tetrameric. In both cases, TTR sediments as a single species with an *S* valve of 3.7 ± 0.1 (Supporting Information, Figures 3 and 4) corresponding to tetrameric TTR. It is clear that *N*-phenyl phenoxazine **4** stabilizes the TTR tetramer under acidic conditions where it would otherwise efficiently dissociate to monomers and self-associate into oligomers, ultimately forming amyloid filaments and fibrils.[10,32,33] The off rate of the inhibitor must be very slow relative to the on rate and the rate of tetramer dissociation, as

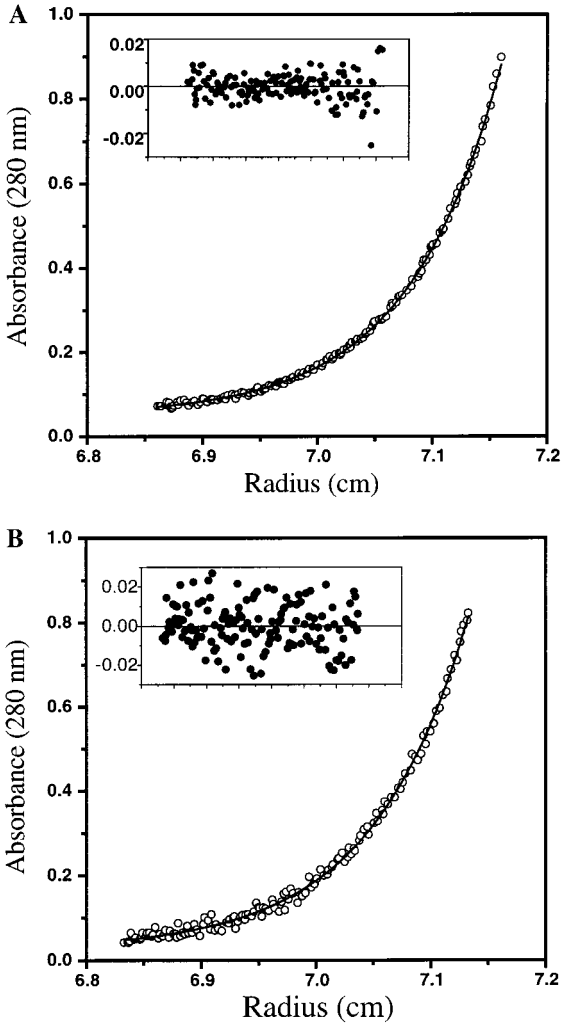

Figure 4. Sedimentation equilibrium analysis of 3.6 μM solutions of WT TTR (A) and L55P TTR (B) in the presence of **4** (7.2 μM) at pH 4.4 (maximal fibril formation conditions) after 72 h and 7 days of incubation, respectively. The solid line was derived from fitting the absorbance vs the radial position data to Equation II for a homogeneous tetrameric species bound to 2 equiv of **4**. The residual difference (residuals) between the experimental data (○) and the fit at each data point is shown in the inset.

fibril formation does not noticeably increase when a 72 h time point is compared to a 168 h time point.

Solid State Characterization of Inhibitor 4. The bis-methyl ester of phenoxazine **4** (compound **22**) was crystallized to characterize its preferred conformation. Not surprisingly, the *N*-phenyl ring is oriented roughly perpendicular (86°) to the plane of the phenoxazine ring system, Figure 1D, Supporting Information Figures 5 and 6. The phenoxazine ring system itself is nearly flat, exhibiting only a 11.3° angle between the two phenyl rings composing the tricyclic ring system. The N^{10} bond angles (118.2°, 118.9°, 119.6°) and planar orientation of the attached ligands are consistent with sp^2 N^{10} hybridization (Supporting Information Tables). Knowing the preferred conformation allows for a more thorough evaluation of the TTR·(**4**)$_2$ cocrystal structure discussed below.

The TTR·(4)$_2$ X-ray crystal Structure. The 1.9 Å resolution structure of **4** bound to both binding sites within TTR demonstrates that the *N*-phenyl phenoxazine binds in its low-energy conformation in two symmetry equivalent modes, Figure 5A. Both were in good agreement with the unbiased 2 $|F_o| - |F_c|$ Φ_{calc} omit maps phased in the absence of **4**. The tricyclic ring system of **4** spans the entire outer hormone binding cavity of TTR, making van der Waals interactions with the side chains of Thr-106, Lys-15, and Leu-17 in two adjacent TTR subunits simultaneously, Figure 5, A and B. This binding conformation positions one of the carboxylate substituents of **4** in close enough proximity to form a weak hydrogen bond with the ϵ-ammonium group of Lys-15 (O4:Nϵ distance 3.3 Å), Figure 5B. The second carboyxlate group is 3.2 Å from the carboxylate of Glu-54 allowing for a possible weak hydrogen bond, assuming that one of the carboxylate groups is protonated at pH 7.4, Figure 5B.

The binding of the *m*-CF_3-substituted phenyl ring of **4** displaces the ordered H_2O molecule found in the innermost binding cavity of the apo TTR structure. Hydrophobic interactions are observed between *m*-CF_3 group of **4** and the second most interior halogen binding pocket, delineated by the side chains of Leu-17, Leu-110, and Thr-119, Figure 5B, Supporting Information Figure 8. Binding of **4** causes the hydroxyl side chains of all four Ser-117 residues to rotate 120° toward the interior of the TTR tetramer. The rotated Ser-117 side chains appear to form the intersubunit H-bonding interactions observed in the TTR·$(Flu)_2$ structure, but not observed in the structure of apo TTR, Figure 5B.[33] The *m*-CF_3 phenyl substructure of **4** does not bind as deeply into the inner binding cavity as the corresponding group in the TTR·$(Flu)_2$ structure (carbon atom of CF_3 group is translated outward by 2.5 Å), compare Supporting Information Figures 7 and 8.[33]

Discussion

The focus of this study was to use a structure-based ligand design strategy to produce small molecule inhibitors against WT and L55P transthyretin amyloid fibril formation. The extreme amyloidogenicity of L55P TTR and the poor ligand binding characteristics generally exhibited by this variant represent a demanding target for scrutinizing potential small molecule inhibitors (see introduction). The design criteria outlined in the results section were tested by synthesizing 15 *N*-phenyl-4,6-phenoxazine dicarboxylates.

The experimental results summarized in Table 1 and Figure 3, A and B, demonstrate that several *N*-phenyl phenoxazines are very good inhibitors against both WT and L55P amyloid fibril formation *in vitro*. Phenoxazines **4** and **5** are excellent at inhibiting both WT and L55P TTR amyloid fibril formation. The ability of **4** and **5** to completely inhibit L55P fibril formation at a concentration of 7.2 μM is unprecedented, Figure 3B. The analogue studies outlined in the results section demonstrate that the entire structure of **4** and **5** appear to be required for inhibitor efficacy. That the substituted *N*-phenyl ring is essential can be discerned from the poor activity of phenoxazines **19** and **17**. Inhibitor **6** demonstrates that bis-meta substitution does not improve activity; instead, activity decreases. An analogue of **6** lacking both carboxylates is also a very poor inhibitor, even at a concentration of 36 μM, demonstrating the importance of the electrostatic interactions. The numerous active meta- and para-substituted *N*-phenyl-4,6-phenoxazine dicarboxylates (e.g., **4**−**10**, Table 1) suggest that additional manipulation of this *N*-phenyl ring could yield inhibitors that are even more potent.

Phenoxazine **4** binds to WT TTR with a dissociation constant of 79 ηM, 2-fold higher than that exhibited by Flu, whereas the dissociation constant for Flu and **4** (237 ηM) binding to the second TTR site are within error, Table 2A. Hence, it is not surprising that Flu and **4** exhibit very similar efficacy as WT TTR amyloid fibril inhibitors, since the concentrations employed (3.6 or 7.2 μM) are significantly higher than the dissociation constants, owing to the concentration of TTR in human plasma

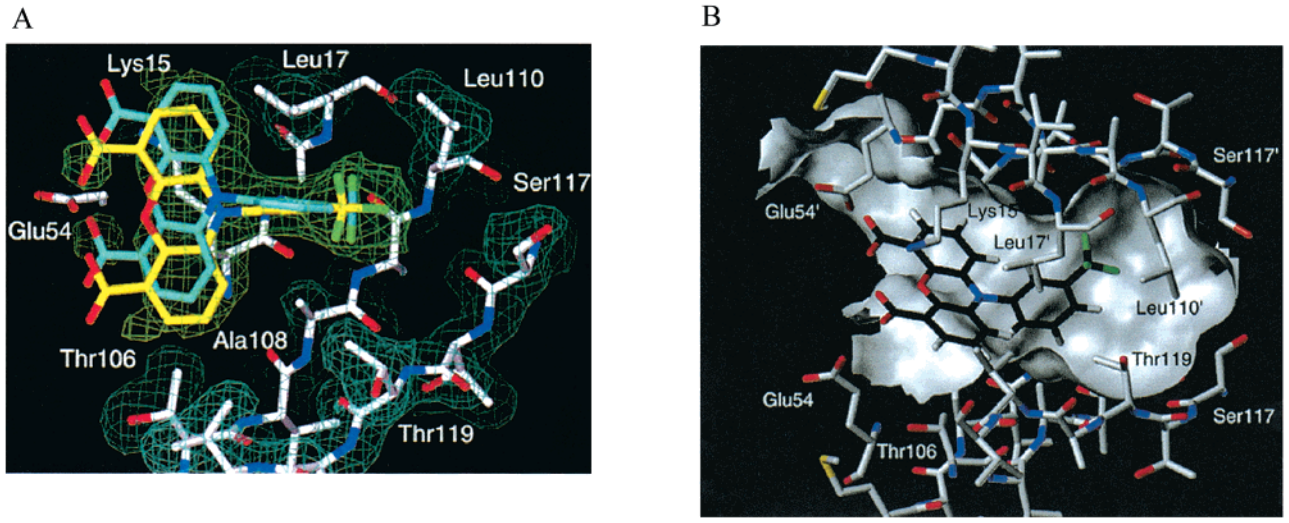

Figure 5. Structural representations of the X-ray structure of **4** bound to one of the two C_2 symmetrical TTR hormone binding sites. (A) Framework model representation of the two symmetry equivalent binding modes of **4** (one where C atoms are depicted in yellow and the other in aqua). Only residues from one subunit of TTR that form the binding cavity are displayed with their 2 $|F_o| - |F_c|$ Φ_{calc} electron density in cyan. The symmetry related binding modes of **4** fit nicely into the final 2 $|F_o| - |F_c|$ Φ_{calc} electron density in green. In the framework model, oxygen atoms are in red, nitrogen atoms in blue, and fluorine in green. The protein ligand interactions are described in the text. (B) A molecular surface representing a cut away view of one of the TTR binding pockets (shown in gray) occupied by **4** in one of its symmetry equivalent binding modes. Ligand **4** is depicted in stick format using the same color scheme as in A, with the exception that carbons are in black. The binding site is formed by two adjacent TTR monomers related by a C_{2z} operation (see Figure 1A). Residue side chains undergoing rearrangement upon binding **4** include Ser-117, Thr-119, and Lys-15. The *m*-CF_3 substituted phenyl ring of Flu is translated 2.5 Å deeper into the innner binding sub-site that the analogous substructure in **4** (see Supporting Information Figures 7 and 8 for a comparison). Interactions of **4** with the periphery of the TTR binding site likely maximize hydrophobic interactions and allow some interactions of **4** with D strand residues such as Glu-54, which may prevent the putative C-strand-loop-D-strand rearrangement that leads to the formation of the amyloidogenic intermediate.

(3.6 μM). The binding of **4** to L55P TTR is characterized by a 5-fold increase in K_{d1} (357 ηM) and 1.5-fold increase in K_{d2} (1050 ηM) relative to Flu, Table 2A. Yet, phenoxazine **4** is a better inhibitor than Flu when used at a concentration of either 3.6 or 7.2 μM. This apparent conundrum can be rationalized by considering the possibility that inhibitor efficacy results from both ground-state and transition-state effects. The possibility that **4** raises the free energy of the transition state associated with the tetramer to amyloidogenic monomer transition in addition to stabilizing the L55P TTR·$(\mathbf{4})_2$ ground state is not unreasonable based on the Hammond Postulate, which predicts that the transition state structure would be tetramer-like. Hence ligand binding could destabilize the transition state, Figure 6. In addition, it is possible that the binding constants of Flu and **4** could reverse their relative affinities over the pH range of 7.6−4.4, providing an alternative explanation for the lack of correlation between binding and inhibitor efficacy, the latter limit being the pH where the inhibitor evaluations were made (37 °C) and the former where the binding constants were measured by ITC experiments (25 °C). Unfortunately, dissociation and conformational changes leading to amyloid fibril formation preclude analyzing binding at pHs lower than 7.6 (a detailed summary of the technical problems can be found elsewhere).[32]

The 1.9 Å X-ray crystal structure of phenoxazine **4** bound to both binding sites in TTR reveals that the simple design criteria used to envision the *N*-phenyl phenoxazine inhibitors were by in large correct (see results section). The structure confirms that the molecular surface of **4** nicely complements the van der Waals surface of the TTR binding cavity. The phenoxazine ring system occupies the outer thyroid hormone binding cavity while the *m*-CF_3-substituted phenyl ring occupies the inner TTR binding cavity. One of the two carboxylates comprising **4** is close enough to make a favorable electrostatic interaction with the ϵ-ammonium side chain of Lys-15. As is typically the case in structure-based ligand design, the structure of the complex revealed some unexpected features as well. Phenoxazine **4** does not enter the hormone binding channel as deeply as Flu, suggesting that further modifications of the substructure projecting from N^{10} into the inner sub-site may improve binding and efficacy, compare Supporting Information Figures 7 and 8. On the other hand, deeper penetration of **4** could be deleterious, as the high efficacy may be a direct result of interactions between the phenoxazine ring system and the outer binding cavity of TTR (vide infra). The other unexpected feature emerging from the TTR·$(\mathbf{4})_2$ structure is that one of the carboxylates of **4** is in close enough to share a proton with Glu-54; however the energetic significance of this potential H-bonding interaction for inhibitory activity is not yet known.

The molecular recognition event between TTR and **4** mediated by complimentary van der Waals, hydrophobic, and electrostatic interactions appears to prevent tetramer dissociation and the linked conformational changes associated with TTR amyloid formation (via ground-state stabilization and possible transition state destabilization, see Figure 6).[27,46,47] Due to the increased size of the 4,6-phenoxazine dicarboxylic acid relative to the anthranilic acid substructure of Flu, **4** is able to make van der Waals contacts with both subunits of TTR composing the binding cavity simultaneously. The isothermal titration calorimetry data in Table 2 also suggest that inhibitor **4** and Flu interact differently with TTR. The fact that the entropy of

(45) Andrea, T. A.; Cavalieri, R. R.; Goldfine, I. D.; Jorgensen, E. C. *Biochemistry* **1980**, *19*, 55−63.
(46) Kelly, J. W.; Lansbury, P. T. J. *Amyloid: Int. J. Exp. Clin. Invest.* **1994**, *1*, 186−205.
(47) Blake, C. C. F.; Serpell, L. C.; Sunde, M.; Sandgren, O.; Lundgren, E. In *A Molecular Model of The Amyloid Fibril*; Blake, C. C. F., Serpell, L. C., Sunde, M., Sandgren, O., Lundgren, E., Eds.; John Wiley and Sons: Chichester, 1996; Ciba Symposium Vol. 199, pp 6−21.

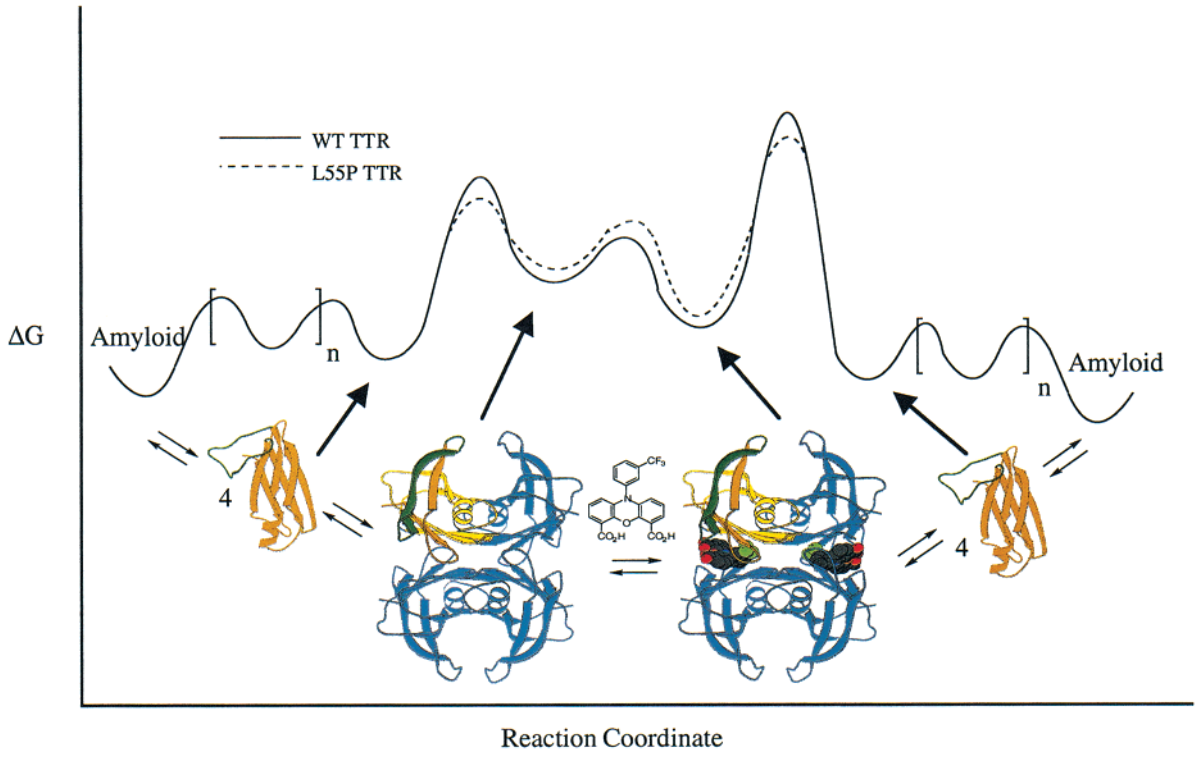

Figure 6. Free energy reaction coordinate diagram for the formation of the monomeric amyloidogenic intermediate from WT and L55P TTR (pH 4.4) in the presence (right side) and absence (left side) of **4**. From previous studies we know that the WT tetramer dissociation is associated with a high activation barrier (rate-determining step), which is decreased in the case of the L55P mutation.[26] We also know from previous studies that the WT tetramer is more stable that the L55P variant which is reflected in the free energy reaction coordinate diagram.[8,9,11,25] Ligand binding is known to decrease the free energy of the TTR·(**4**)$_2$ complex, making the activation barrier for L55P and WT TTR fibril formation more unfavorable. If the transition-state structure mirrors the tetramer, as expected (Hammond Postulate), the T.S. energy will go up due to the binding of **4**. Tetrameric TTR is depicted in ribbon format with one of four identical subunits colored in gold bound to 2 molecules of **4** represented in space-filling format (CPK). Note that the two exterior strands (the C and D strands shown in dark green) are presumed to melt away from the hydrophobic core upon dissociation of tetrameric TTR yielding the six-stranded amyloidogenic intermediate which ultimately affords amyloid by self-assembly.

binding of **4** to TTR is favorable, while the entropy of Flu binding is unfavorable can, in part, be attributed to the ability of **4** to displace more H_2O from the hydrophobic cavity, Table 2B. In addition, there is a minimal conformational entropy penalty associated with the binding of **4** because it binds in its lowest-energy conformation as discerned by a comparison of the crystal structure of **22** and the bound conformation of **4** in the TTR·(**4**)$_2$ structure, compare Figures 1D and 5A. The conformational changes occurring in TTR (involving Ser-117 and Thr-119; vide infra) are very similar to those mediated by Flu binding to TTR. Hence, the observed differences in the enthalpy and entropy of ligand binding likely result because of the different degree of penetration and molecular interactions between **4** and TTR, and are not likely to be due to ligand-induced conformational changes within TTR.

The non-cooperativity associated with the binding of **4** to TTR relative to the negatively cooperative binding of Flu may be a manifestation of the degree to which the ligands penetrate the inner binding cavities. The deeper penetration of Flu is envisioned to make solvent displacement more difficult upon occupancy of the second binding site. Ligands such as T4 and Flu which bind deep into the inner binding cavity exhibit negative cooperativity, as opposed to compound **4** which binds in the periphery of each cavity non-cooperatively. This is the first structural clue that the degree of negative cooperativity may be linked to the degree of difficulty associated with the H_2O displacement from the inner TTR cavity upon occupancy of the second ligand binding site.

It is clear from both the WT-TTR·(**4**)$_2$ and WT-TTR·(Flu)$_2$ structures that these inhibitors mediate TTR conformational changes that may be important for preventing dissociation and misfolding required for fibril formation (vide infra). Even though the binding of **4** to TTR is not as energetically favorable as Flu binding, the conformational changes mediated by **4** may be different enough to make fibril formation more difficult. The TTR conformational changes involving the Thr-119 and Ser-117 side chains mediated by ligand binding not only allow for increased van der Waals contacts between **4** and the protein, but they also may stabilize the TTR tetramer and possibly destabilize the transition state associated with misfolding. Phenoxazine induced conformational changes in TTR also facilitate the formation of a hydrogen bond between the Oγ atom of Thr-119 to an ordered H_2O molecule, which in turn is hydrogen bonded to the carbonyl oxygen of Asp-18 on an adjacent TTR subunit. The binding of **4** and Flu lead to a similar desolvated hydrogen bonding network involving the Ser-117 residues on adjacent TTR subunits (see Introduction).[33] Further mutagenesis/biophysical studies are necessary to be confident that these changes are energetically important and to address whether they effect the ground state, the transition state, or both.

Conclusions

Starting with the 2.0 Å X-ray crystal structure of the transthyretin·(flufenamic acid)$_2$ complex, a structure-based ligand design strategy was utilized to conceive *N*-phenyl phenoxazine transthyretin (TTR) amyloid fibril inhibitors. Fifteen *N*-phenyl phenoxazines were chemically synthesized, two of which proved to be excellent WT and L55P TTR amyloid fibril inhibitors. The structure of one of the two most active phenoxazines, **4**, bound to TTR was solved to a resolution of

1.9 Å. *N*-phenyl phenoxazine **4** binds similar to the orientation anticipated, although not as deeply into the channel as expected. Ultracentrifugation studies demonstrate that **4** blocks the first step of TTR amyloid fibril formation, that is, tetramer dissociation to the alternatively folded monomeric amyloidogenic intermediate. It is clear that **4** functions in part by stabilizing the normally folded tetramer through formation of the TTR·$(\mathbf{4})_2$ complex, which in turn increases the activation energy for tetramer dissociation. The data also suggest that **4** destabilizes the transition state associated with TTR dissociation to the monomeric amyloidogenic intermediate, Figure 6. The ability to inhibit transthyretin amyloid fibril formation in vitro is extremely important for enabling a test of the validity of the amyloid hypothesis in vivo. The phenoxazine inhibitors **4** and **5** put us one step closer to that goal.

Acknowledgment. The authors gratefully acknowledge primary financial support from the National Institute of Health (R01 DK46335-01) and secondary support from The Skaggs Institute of Chemical Biology, The Lita Annenberg Hazen Foundation, the Donald and Delia Baxter Foundation, and the Welch Foundation (T.K., J.S.). We thank Mr. Scott Peterson, Ms. Traci Walkup, Dr. Edward Koepf, and Ms. Linda Woo for assistance with protein expression, Mr. Hans Purkey for carrying out ITC studies on Flu binding to WT and L55P TTR and for dissection of the energetics involved, and Mr. Hilal A. Lashuel, Dr. Vibha Oza, and Dr. Prakash Raman for helpful discussions involving analytical ultracentrifugation and chemical synthesis.

Supporting Information Available: Included are the ITC data and curve fits for **4** binding to WT and L55P TTR in Figures 1 and 2, respectively; sedimentation velocity data on WT and L55P TTR in the presence of 7.2 μM **4** at pH 4.4 in Figures 3 and 4, respectively; ORTEP and stereoviews of **22** in Figures 5 and 6, respectively; comparison of the degree of penetration of Flu vs **4** into the TTR ligand binding site in Figures 7 and 8, respectively; and Tables of crystallographic data for **22** on several pages (PDF). This material is available free of charge via the Internet at http://pubs.acs.org.

JA993309V